The Life-Cycle of the Jet-Driven Shear-Flow Dynamo

B. Tripathi[1,2,*], A.E. Fraser[3], P.W. Terry[1], E.G. Zweibel[1], M.J. Pueschel[4,5,6]

[1]University of Wisconsin–Madison, Madison, Wisconsin 53706, USA.

[2]Columbia University, New York 10027, USA.

[3]University of Colorado, Boulder, Colorado 80309, USA.

[4]Dutch Institute for Fundamental Energy Research, 5612 AJ Eindhoven, The Netherlands.

[5]Eindhoven University of Technology, 5600 MB Eindhoven, The Netherlands.

[6]Department of Physics & Astronomy, Ruhr-Universität Bochum, 44780 Bochum, Germany.

[*]Author to whom correspondence should be addressed: bt2693@columbia.edu

(Dated: February 11, 2026)

Abstract

Shear flows can generate and sustain large-scale, quasi-cyclic, self-organized magnetic fields in three dimensions via a process called the dynamo. Here, the essential steps of a dynamo process are identified and confirmed using energy transfer analyses of turbulence driven by the Kelvin–Helmholtz (KH) instability. The dynamo cycle begins with an (x, y)-averaged mean horizontal shear-flow $U_x(z)$, which is maintained externally. The KH instability, which represents the x-varying fluctuations, nonlinearly excites x-invariant, y-varying vertical flows and magnetic fields—labeled **u**-rolls and **b**-rolls. These vertical perturbations are strained by the mean shear flow to generate horizontal x-invariant, y-varying flows and magnetic fields. These are labeled zonal jets and zonal magnetic fields. The zonal jets then stretch the **b**-rolls, creating an (x, y)-averaged mean horizontal magnetic field. The z-gradient of the mean magnetic field saturates when the **u**-rolls advect the mean magnetic field vertically. The zonal jets are sustained by energy transfer from the primary KH instability of the mean shear flow. These processes are robust under key parameter variations. This dynamo cycle explains the operation mechanism of a recently confirmed mean-field dynamo theory—the mean-vorticity effect—applicable in a host of plasmas.

I. INTRODUCTION

Dynamo action—the generation of magnetic fields and their sustenance against resistive dissipation in magnetofluids and plasmas—is a long-standing research topic [1–19], and is traditionally thought to be driven by helical turbulent fluid motions acting on an imposed large-scale field [1, 5, 6, 18–20]. However, a recent study [21] reported dynamo action even in the absence of an initial large-scale field via a non-traditional mean-field theory—the mean-vorticity effect [22]. This study presented a surprising finding that the dynamo-generated large-scale field is nearly identical in spatial profile to that of the large-scale shear flow. The primary objective of this work is to identify the mechanisms via which the large-scale flow generates the large-scale field, and the mechanisms via which the large-scale field saturates. There exist three broad issues: identification of the chain of steps involved in the dynamo, understanding of the role of the Kelvin–Helmholtz (KH) instability arising from the large-scale shear flow [23], and classification of the steps of the dynamo as they relate to either hydrodynamics or magnetic fields. Since the chain of these complex turbulent processes is not evident in a simple mean-field theory [19], a thorough analysis is required to identify the chain of steps by which the energy in the large-scale shear flow accumulates in the large-scale field.

To understand the chain of steps in a dynamo that generates large-scale field, one needs to analyze the nonlinear energy transfer channels by which the large-scale field receives energy from certain entities and returns it to other entities. The ultimate energy source for the large-scale-vorticity-driven dynamo [22] is the large-scale shear flow, which then becomes linked to a large-scale field. This chain of links connecting the large-scale flow and large-scale field can in principle involve a large number of nonlinear interactions, although in practice the number is often small. Identification of these interactions requires detailed analyses of magnitude and direction of nonlinear energy transfers.

The linear instability of a shear flow deposits energy in large-scale fluctuations [23], which may directly induce a dynamo—or, the linear instability may nonlinearly excite fluctuations at other scales, which may then induce a dynamo. Usually, the large-scale instability-related fluctuations break down into small scales, when the unstable shear flow relaxes toward a stable configuration due to continual energy extraction from the freely-evolving shear flow [24]. Under such a scenario, large-scale shear flow rapidly generates [25–28] velocity and magnetic

fields at small scales—until the turbulence has decayed and the dynamo action has stopped. By this time, the slowly-evolving large-scale magnetic fields may not have been generated. However, when the large-scale shear flow is forced so as to maintain its initial unstable equilibrium — a natural scenario in various astrophysical environments [29–34] — turbulent eddies exist at large instability scales as well as at small scales. The large-scale eddies continuously extract energy from the large-scale shear flow, nonlinearly distribute energy to other scales, and thus sustain quasi-stationary turbulence with a possible continuous dynamo action, allowing the slow emergence of large-scale magnetic fields. Addressing whether these large-scale magnetic fields are a direct product of large-scale instability-generated fluctuations or a byproduct of small-scale turbulence requires an understanding of turbulent energy transfers.

The operation of the dynamo driven by the KH instability involves a chain of steps, some of which are purely hydrodynamic and others involve magnetic fields. The linear instability of the large-scale shear flow can nonlinearly excite other scales of flow and magnetic fields, in particular both small and large. For example, a recent three-dimensional *hydrodynamic* KH-driven turbulence study [35] showed the emergence of large-scale nonlinear fluctuations that do not vary in the direction of the large-scale shear flow but vary in the direction orthogonal to the two-dimensional shear-flow plane. These inherently three-dimensional fluctuations have zero linear growth rate; nonetheless, they are nonlinearly excited by the instability to large amplitudes [35]. These nonlinear, hydrodynamic, anisotropic, large-scale fluctuations appear in the form of jets [35, 36] — similar to zonal flows in fusion plasmas and planetary atmospheres [37–39]. The large-scale jets have intrinsically different properties from those of the nonlinear fluctuations at small, dissipative scales. Among these properties, the following critically impact the dynamo: First, the energy-containing jets at large-scales strongly stretch fluctuation fields compared to that by the inertial-range eddies, which are less-energetic (in the presence of large-scale coherent structures, the turbulence spectrum falls off very rapidly compared to the slow Kolmogorov spectrum limited to a homogeneous turbulence). Second, alignment between flow and fields—in addition to their amplitudes—is crucial for a dynamo action: The large-scale jets stretch fluctuation fields coherently [40], whereas the small-scale turbulent flows stretch fields randomly [41, 42]. Third, the jets directed along the mean flow are exact solutions to the nonlinear (magneto-)hydrodynamic equations, similar to the Elsässer fields [43]. This exact-soluble property makes these jets

resilient to perturbations. While these features of the jets are favorable for large-scale dynamo, the magnetic fields may back-react on the jets via the Lorentz force. Hence, if the shear-flow dynamo is to be better-understood, an analysis of the interaction between the jets and magnetic fields is crucial.

To address the foregoing issues, we perform an ensemble of high-resolution three-dimensional instability-driven magnetohydrodynamic (MHD) turbulence simulations using spectral methods [44]. We conduct comprehensive energy transfer analyses to track the magnitude and direction of energy transfer in wavenumber-triad interactions [45].

The chief finding of this work is the identification of nonlinear interactions of turbulent flow and magnetic fields that take energy away from the large-scale shear flow and ultimately deposit it in the large-scale magnetic field; the latter two are not directly coupled but are indirectly coupled via turbulence. The steps for this indirect coupling operate in the following way: The large-scale shear flow—which we maintain externally and continuously—excites the KH instability; the KH instability induces hydrodynamic jets; the jets create large-scale magnetic fields via turbulent field-line stretching; and the large-scale fields saturate when the horizontal jets create large-scale fields at a rate that is balanced approximately by the rate at which the large-scale fields are turbulently transported by fluctuating vertical flows. That is, the rate of field-gradient steepening by jets balances the rate of field-gradient flattening by turbulence. This series of steps produces a dynamically-evolving dynamo. Because the jets are nonlinearly driven, this process is observed to develop in the turbulent phase over very long time scales relative to the short linear KH growth time. When the large-scale flow is not maintained, turbulence decays quickly before the reported dynamo emerges.

This article is organized in the following way. Section II describes the system setup. Section III presents an overview of the dynamo cycle. Detailed confirmation of the dynamo cycle is presented in Sec. IV. In Sec. V, the different elements of the dynamo are measured by varying control parameters. Broader implications of this work are discussed in Sec. VI before concluding in Sec. VII.

II. MHD-KH DYNAMO SETUP

Throughout this article, we label the (x, y)-averaged flow as the *mean* (large-scale) flow. Similarly, we label the (x, y)-averaged magnetic field as the *mean* (large-scale) field.

A. Governing equations

We evolve the flow $\mathbf{u}$ and magnetic field $\mathbf{b}$ by solving three-dimensional (3D) incompressible MHD equations [48]

$$\partial_t \mathbf{u} - \nu\nabla^2\mathbf{u} + \nabla P = -\mathbf{u}\cdot\nabla\mathbf{u} + \frac{\mathbf{j}\times\mathbf{b}}{\rho} + \mathbf{f}, \tag{1a}$$

$$\partial_t \mathbf{A} - \eta\nabla^2\mathbf{A} + \nabla\Psi = \mathbf{u}\times\mathbf{b}, \tag{1b}$$

$$\nabla\cdot\mathbf{u} = 0, \tag{1c}$$

$$\nabla\cdot\mathbf{A} = 0, \tag{1d}$$

$$\mathbf{b} = \nabla\times\mathbf{A}, \tag{1e}$$

$$\mathbf{j} = \frac{\nabla\times\mathbf{b}}{\mu_0}, \tag{1f}$$

where ∂_t and ∇ represent differentiation with respect to time and 3D space, respectively; ν and η are kinematic viscosity and electric resistivity, respectively; P is the fluid pressure per unit density ρ; and μ_0 is the vacuum permeability.

We write $\mathbf{b}$ in terms of the vector potential $\mathbf{A}$. This form (1e) ensures that the magnetic field $\mathbf{b}$ is always divergence-free. Equation (1d) is the Coulomb gauge. The electric current density $\mathbf{j}$ is given by Ampere's law (1f). The externally applied force per unit mass of the fluid is given by $\mathbf{f}$. Forcing in the magnetic induction equation is avoided [6], which allows us to focus on the KH-instability-driven processes.

We simulate 3D MHD dynamo with both kinds of initial conditions: with an initial uniform mean magnetic field $\mathbf{B}_0$ [49] and without an initial uniform mean magnetic field.

B. Flow profiles and non-dimensionalization

To investigate the dynamo driven by the KH instability, we consider a mean unstable shear-flow [23] $\mathbf{U}_0{=}U_0\tanh(z/a)\hat{\mathrm{e}}_x$, where $\hat{\mathrm{e}}_x$ is the unit vector along x. Here, U_0 is the flow-amplitude of the mean shear layer, whose half-width is a.

Throughout this paper, U_0 and a are used to non-dimensionalize all parameters, e.g., the fluid Reynolds number is $Re{=}aU_0/\nu$, and the magnetic Reynolds number is $Rm{=}aU_0/\eta$; the magnetic Prandtl number is $Pr{=}Rm/Re$. Note that these Reynolds numbers, defined with respect to the initial laminar shear flow [29] (before the flow becomes turbulent), are not

the same as the turbulent Reynolds number defined by $Re_{\rm turb} = u_{\rm rms} l_{\rm rms}/\nu$, where $u_{\rm rms}$ is the root-mean-square turbulent velocity, $l_{\rm rms}$ is the length scale of the characteristic energy-containing eddy, and ν is the kinematic viscosity. In this work, the energy-containing eddies are found to be of the size of the domain scale L, and $u_{\rm rms}$ to be of the order of U_0. Since $L \gg a$, we find that $Re_{\rm turb}$ is substantially larger than Re.

The dynamo in the current paper is driven by the Kelvin–Helmholtz (KH) instability of the mean shear flow with amplitude U_0. Note that the growth rate of the KH instability is linearly proportional to U_0. We non-dimensionalize all quantities in this article using two parameters: U_0 and the half-width a of the shear layer, given by $U_x(z) = U_0 \tanh(z/a)$. Hence, we measure length in units of a, speed in units of U_0, and time in units of a/U_0. When these normalizations are used, U_0 is no longer a free, separate parameter. Under such a scenario, U_0 appears only in two places in the governing MHD equations: In the momentum equation, U_0 appears in $Re = aU_0/\nu$, and in the magnetic induction equation, U_0 appears in $Rm = aU_0/\eta$. One can interpret variations in Re and Rm in two different ways. One can either think of variations in Re and Rm as variations in U_0, where ν and η are kept fixed. Another way to interpret the variations in the given Re and Rm is that U_0 is fixed, and ν and η are varied.

We emphasize that, if U_0 is zero, the shear flow does not exist; in the absence of this unstable shear flow, the Kelvin–Helmholtz instability disappears; in the absence of the KH instability, there is no turbulence, no jets, and hence no dynamo in the current problem. This behavior arises because we do not rely on an external stirring to drive turbulence, which is generally considered in dynamo studies with a local shear flow that has a linear profile (e.g., [46]); such linear shear flow is stable to the KH instability (the KH instability requires a non-zero second derivative in the flow profile). Here, we consider a nonlocal shear flow whose profile has a non-zero second derivative. Since the mean shear flow itself is unstable, it drives linear instability at large scales; this large-scale instability then nonlinearly excites other scales, including the small scales. Hence, an additional external turbulence stirring is not required. The instability itself stirs all scales nonlinearly. Hence, we focus on the natural excitation of turbulence by the KH instability.

C. Spectral bases, initial perturbations, boundary conditions, and forcing

The simulation domain size $L_x \times L_y \times L_z$ is measured in units of a; compared to a, a large domain $L_x = L_y = L_z = 10\pi$ is used [24]. Since z is the direction of inhomogeneity (due to the mean shear flow), we expand the state vector corresponding to flow and magnetic fields in z in Chebyshev polynomials.

We seed small-amplitude, multi-mode, divergence-free perturbations in flow and fields, and we randomize the phases of the perturbations at every wavenumber (k_x, k_y). To create these general initial perturbations free of divergences, we first express perturbations in the flow as $\mathbf{u} = \nabla \times \mathbf{C}^u$, and then prescribe a perturbation in the vector $\mathbf{C}^u$, whose j-th component is

$$C_j^u = \hat{\mathrm{e}}_j \, D \, \mathrm{e}^{-\frac{z^2}{\sigma^2}} \Bigg(\sum_{0<|k_x|<k_x^*} \mathrm{e}^{ik_x x} |k_x|^\alpha \mathrm{e}^{i\theta_j(k_x)} \delta_{k_y,0} + \sum_{0<|k_y|<k_y^*} \mathrm{e}^{ik_y y} |k_y|^\alpha \mathrm{e}^{i\theta_j(k_y)} \delta_{k_x,0} + \sum_{\substack{0<|k_x|<k_x^* \\ 0<|k_y|<k_y^*}} \mathrm{e}^{ik_x x} \mathrm{e}^{ik_y y} |k_x|^\beta |k_y|^\beta \mathrm{e}^{i\theta_j(k_x)} \mathrm{e}^{i\theta_j(k_y)} \Bigg), \tag{2}$$

where D is the amplitude of the perturbation C_j^u. To create magnetic perturbations $\mathbf{b} = \nabla \times (\nabla \times \mathbf{C}^b)$, we prescribe a similar profile for the vector $\mathbf{C}^b$.

Motivated by our earlier studies on two-dimensional MHD [34, 47, 50] and three-dimensional hydrodynamic shear-flow turbulence [35], we choose a small-amplitude perturbation with $D = 10^{-3}$ to allow a discernible linear evolution of the instability, before it gets nonlinearly modified. To avoid preferential excitation of certain wavenumbers, we require the initial perturbations to have a near-flat spectrum of energy: we take $\alpha = -1$ and $\beta = -1/2$ for the perturbed velocity $\nabla \times \mathbf{C}^u$; we take $\alpha = -2$ and $\beta = -1$ for the magnetic field $\mathbf{b} = \nabla \times (\nabla \times \mathbf{C}^b)$. We use different random phases θ_j for flow and fields at different wavenumbers. The cut-off wavenumbers $k_x^* = k_y^*$ for the initial perturbations are $16k_{\min}$, where $k_{\min} = 2\pi/L$. The properties of saturated turbulence, however, are independent of these initial choices: We have reproduced statistically the same results using other choices of initial conditions. Here, we choose $\sigma = 2$ (in terms of a). The initial perturbations in velocity and magnetic fields are divergence-free because they are given by $\mathbf{u} = \nabla \times \mathbf{C}^u$ and $\mathbf{b} = \nabla \times \mathbf{A} = \nabla \times (\nabla \times \mathbf{C}^b)$; for self-consistency, we explicitly compute the initial pressure P by numerically solving the Poisson's equation $\nabla^2 P = \nabla \cdot \{-(\mathbf{u} \cdot \nabla)\mathbf{u} + (\nabla \times \mathbf{b}) \times \mathbf{b}\}$,

which is obtained by taking divergence of the momentum equation. Similarly, we explicitly compute the initial scalar function Ψ by numerically solving the Poisson's equation $\nabla^2\Psi = \nabla \cdot (\mathbf{u} \times \mathbf{b})$, which is obtained by taking divergence of the magnetic induction equation. These explicit Poisson's equations are numerically solved using Dedalus.

In many astrophysical systems and fusion plasma devices where the KH instability arises, a large-scale velocity gradient exists in the radial direction. For example, when two merging neutron stars approach each other, their surfaces touch each other at first. In this process, the azimuthally directed flows have variations in the radial direction (connecting the centers of the binary stars) [63]. This article, therefore, considers a non-periodic boundary condition, applicable in the radial direction. Furthermore, unlike the azimuthal and latitudinal or vertical directions, the radial direction in stars, accretion flows, and galaxies is non-periodic. Additionally, boundary conditions are known to play a critical role in many dynamo studies. Hence, it is useful to study the properties of dynamos in bounded, non-periodic domains.

In this work, we employ periodic boundary conditions in the x and y axes. Along the z-axis, where the mean flow is reversed, we use physical boundary conditions: perfectly conducting, no-slip walls that co-move with the flow at the top and bottom $z = \pm L_z/2$. That is, at the boundaries, $A_x = A_y = \Psi = 0$ (equivalently, $j_x = j_y = b_z = 0$), $u_y = u_z = 0$, and $u_x = \pm 1$ (in units of the amplitude U_0). In simulations where a uniform mean magnetic field is present in the initial conditions, the above magnetic boundary conditions $A_x = A_y = \Psi = 0$ are applied to the the remaining magnetic fields. We have performed simulations with extended domains in z and have reproduced similar results of magnetic field evolution.

To focus on the KH-driven dynamo, we maintain the unstable mean flow—by continuously forcing the instantaneous x-directed mean flow toward its initial unstable profile with the force $\mathbf{f} = f_x \hat{\mathrm{e}}_x$, which has the form

$$f_x = \frac{\langle u_x(t)\rangle_{x,y} - \langle u_x(t{=}0)\rangle_{x,y}}{\tau_{\mathrm{f}}} + F_0, \tag{3}$$

where $\langle u_x(t)\rangle_{x,y}$ represents instantaneous x-directed flow that is averaged in x and y. The term F_0 in Eq. (3) is insignificant and merely removes the viscous relaxation of the mean shear flow at $t = 0$; this removal helps to attain a true initial MHD equilibrium, with $F_0 + \nu\nabla^2\langle u_x(t{=}0)\rangle_{x,y} = 0$. We note that the first term on the right-hand side of Eq. (3) is not required for the initial linear KH instability. We emphasize, however, that, as the instability extracts energy from the gradient of the mean shear flow and drives a Reynolds-

stress momentum flux, the gradient in the mean flow becomes weak and the mean flow relaxes to a stable configuration. Hence, the instability becomes inactive; turbulence decays; and dynamo becomes inactive. Since the large-scale magnetic fields evolve over a longer time—significantly longer than the KH-instability growth time—the decaying dynamo cannot generate and sustain large-scale magnetic fields. To allow sustained, quasi-stationary dynamo, the first term on the right-hand side of Eq. (3) drives the mean shear flow towards its unstable equilibrium. Hence, the KH instability remains active at all times. The saturated KH instability and the ensuing quasi-stationary turbulence generates and sustains the large-scale magnetic fields. It is this particular purpose for which the first term on the right-hand side of Eq. (3) is included. More details on the forcing function and the physics behind it are given in Appendix A.

The forcing time-scale $\tau_{\rm f}$ is chosen to be adequately short so that the mean flow is continuously replenished before the instability depletes it. The depletion otherwise causes the turbulence to decay and the dynamo to become inactive. The e-folding time of the instability is ≈ 5 (in units of U_0/a); we choose $\tau_{\rm f} = 0.5$. While the considered forcing may not be fully representative of all external drives in every natural system, the chosen forcing profile is general and does maintain large-scale flows that are commonly encountered in various astrophysical environments. These include gravity and convection that continuously generate shear layers in stellar interiors, planetary atmospheres where large-scale shear flows are persistent, the merging of binary neutron stars (BNS) that continuously creates shear layers in between the approaching BNS for an extended time until they fully merge, and secondary KH-unstable shear layers in stars and planets [11, 29–31, 34, 51, 52, 63]. Equation (3) represents a standard forcing that is routinely used in plasma physics and in fluid dynamics as a relaxation operator [30, 32, 33].

To solve Eqs. (1a)–(1f), we use the pseudospectral τ-method in Dedalus [44], with the standard 3/2 de-aliasing factor to control aliasing errors while computing nonlinearities. For time-stepping, linear terms are solved implicitly while nonlinear terms are solved explicitly. We use the 3rd-order, 4-stage Runge–Kutta method (the "RK443" option in Dedalus) [53] for most simulations. For a few simulations, we use the "SBDF2" option in Dedalus; the SBDF2 scheme handles implicit terms using the second-order backwards-difference formula and explicit terms using an Adams–Bashforth scheme [54]. Both time-steppers are found to reproduce similar results. While larger CFL factor is used for preliminary runs balancing

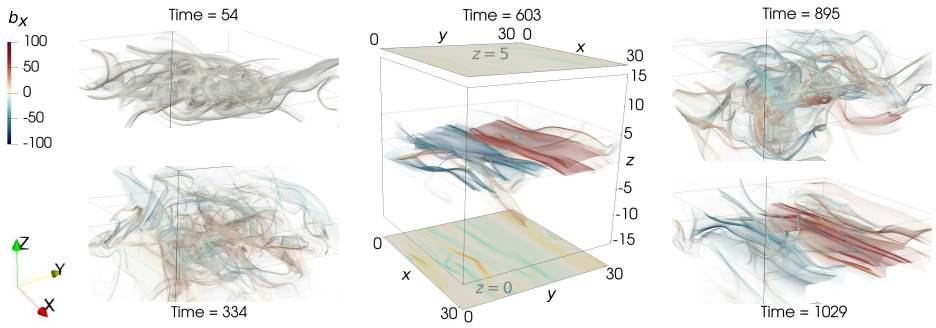

FIG. 1. Evolution of magnetic fields in a KH-instability-driven dynamo simulation, displaying spontaneous transitions between ordered and disordered phases. The field component b_x is shown only in the region of interest, around z=0, where the gradient of the (x, y)-averaged mean flow is the largest. The first panel (time=54, measured in units of a/U_0) shows an early phase, when the KH instability rapidly folds the magnetic field into small-scale structures. The folding of the field continues (time=334), until the large-scale dipolar-in-y fields emerge (time=603). The (x, y)-averaged mean field is reversed in z throughout the nonlinear phase (not seen in these renderings around z=0 where the mean field is close to zero). Over time, the large-scale field and current sheets are disrupted; the system becomes disordered and turbulent, again (time=895). The large-scale field is self-organized and re-generated (time=1029). This quasi-cyclic transition between ordered and disordered phases continues throughout the simulation evolved up to time=12,000. All times are measured in units of a/U_0, where a is the half-width of the shear layer with amplitude U_0. The parameters used are $M_\mathrm{A} = 30$, $\tau_\mathrm{f} = 0.5$, $Re = Rm = 50$, and $\theta = 30°$ (angle between the initial mean flow and the initial mean field).

numerical stability and accuracy, the CFL factor is conservatively set to 0.1 in several production runs, allowing us to obtain higher accuracy and finely resolved temporal dynamics. Simulations show that 128 Fourier modes in x and in y achieve converged dissipation rates for our typical input parameters. Viscous dissipation rates are converged even with lower resolution. We vary the number of modes of Fourier–Fourier–Chebyshev bases from $128^2 \times 512$ to 1024^3 depending on the simulation parameters. All simulations are three-dimensional and are run typically for several hundreds of instability e-folding time.

III. AN OVERVIEW OF THE DYNAMO CYCLE

We present here a summary of detailed turbulent processes that cause the magnetic fields to self-organize into ordered phases, disassemble into chaotic disordered phases, and then reassemble, in a quasi-cyclic manner. These phases are shown in Fig. 1.

After performing comprehensive analyses of an ensemble of 3D MHD KH-driven dynamo simulations, we have identified a dynamo cycle, whose essential steps are summarized in ten elemental steps in Fig. 2. This figure summarizes the principal result of the present article. Each step of the dynamo cycle is briefly explained below. Numerical confirmation of each step is detailed in Sec. IV.

The word "steps" is chosen over the word "components," although both may be used interchangeably. In the fully saturated phase, dynamo features all ten steps, which operate with different time scales. However, examining from $t = 0$, the latter steps cannot operate until the former has occurred. For example, the KH instability must grow exponentially before the jets can form and before mean magnetic fields can be created. It is in this sense (examining from $t = 0$), we prefer to use "steps," because one step must happen first before the occurrence of the next until the dynamo saturates.

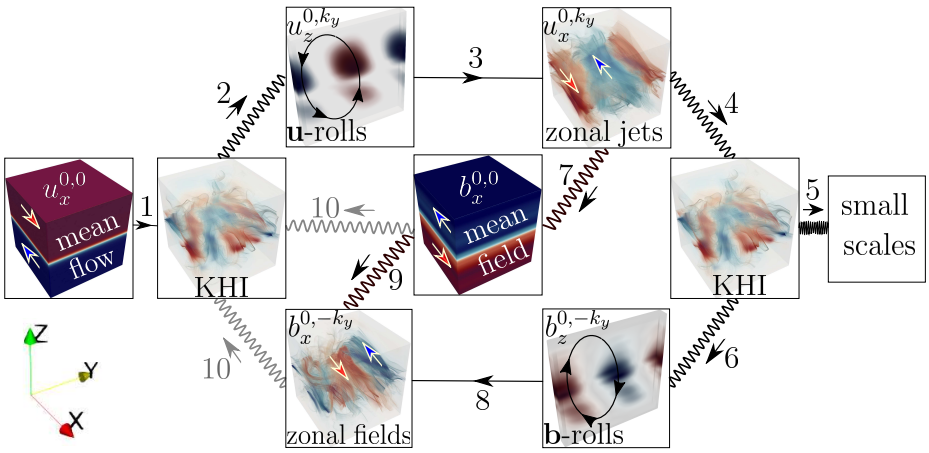

FIG. 2. The life-cycle of the jet-driven shear-flow dynamo using 10 dominant steps. Solid lines represent linear couplings; oscillating curves represent nonlinear couplings. Arrows outside the boxes indicate causality or energy-flow directions. Arrows inside the boxes indicate the direction of flow or field; this direction is indicated by subscripts, e.g, $u_x^{0,0}$. The superscripts represent the horizontal wavenumber k_x, k_y of a given flow or field. All visualizations are shown at the same time in a simulation. Red (blue) represents positive (negative) values. The essential steps of the dynamo cycle are: **1**—The mean shear flow $u_x^{0,0}$ feeds the Kelvin–Helmholtz instability (KHI). **2**—The KHI nonlinearly generates the x-invariant (KH-stable), y-varying vertical flows u_z^{0,k_y}, labeled **u**-rolls and shown in the (y,z)-plane. **3**—The **u**-rolls are stretched by the mean shear flow to form the x-invariant (KH-stable), y-varying horizontal flows u_x^{0,k_y}, labeled zonal jets. The jets are prominent in the 3D rendering of the total turbulent flow. **4**—The zonal jets saturate via nonlinear excitation of turbulent fluctuations in the KH-unstable wavenumber range ($0 < |k_x| \lesssim 1$). **5**—The KHI launches a small-scale energy cascade. Steps **6** and **8** are magnetic analogues of steps **2** and **3**, involving **b**-rolls in place of **u**-rolls. **7**—The zonal jets create a reversed mean field $b_x^{0,0}$ and steepen the mean-field gradient. **9**—The mean field is advected along z by the **u**-rolls, thus flattening the mean-field gradient. **10**—Magnetic fields couple to the KH instability, thus providing saturation of the dynamo. For more details, see Sec. III.

Step 1: The KHI

The mean flow $u_x^{0,0}$ is KH-unstable. Thus, perturbations with wavenumber $0 < |k_x| \lesssim 1$ grow exponentially. The time scale of the KH instability is very short compared to that of other steps.

[As a digressionary remark, we note that perturbations with $k_x = 0$, via the linear physics, neither grow exponentially nor decay exponentially. We distinguish between *perturbation* (Fourier-mode) and *eigenmode*, as the former represents any fluctuation at a given wavenumber, whereas the latter represents a particular eigenfunction of a linear operator at a given wavenumber and corresponds to a particular branch of dispersion relation. The perturbation with $k_x = 0$ is, therefore, not the KH-stable *eigenmode* [55]. The KH-stable *eigenmode*, which decays exponentially via linear physics, requires $k_x \neq 0$, as it exists at the same wavenumber $k_x \neq 0$ where the KH-unstable eigenmode exists. The KH-stable eigenmode is not investigated in this article. While the study of the separate impact of stable and unstable eigenmodes in the dynamo is deferred to future work, analyzing the role of stable modes in dynamo is a fruitful endeavor, because our previous work has shown that they are able to robustly strain magnetic field [34] and that they are significantly excited even in three-dimensional system (previously shown in a hydrodynamical setup) [35].]

Step 2: Generation of x-invariant, y-varying vertical flows (u-rolls)

The KH instability driven by the (x, y)-averaged mean shear flow requires fluctuations to vary along the mean-flow direction, i.e., $k_x \neq 0$. Since the vertical flows $u_z^{k_x=0,k_y}$ do not vary in x but vary in y, they require a purely nonlinear mechanism for their excitation. These x-averaged vertical flows are sliced and shown on the (y, z)-plane in Fig. 2. In the absence of nonlinear drive from the KH-scale fluctuations, the vertical flows decay viscously. These vertical flows are referred to as **u**-rolls here, borrowing a nomenclature from studies of wall-bounded KH-*stable* shear flow [56]. The label *rolls* is appropriate because their spatial structures appear in the form of cylindrical rolls—the axis of the cylinder is along the x-axis. The flows lie on the (y, z)-plane, taking the shape of a roll or an eddy with velocity $(u_y^{k_x=0,k_y}, u_z^{k_x=0,k_y})$. The y-component of the flow is not independent and is related to the z component via the incompressibility condition.

Step 3: Generation of x-invariant, y-varying horizontal flows (zonal jets)

The KH-induced **u**-rolls are stretched by the mean shear flow $u_x^{0,0}$ via the hydrodynamic advection term $u_z^{0,k_y}\partial_z u_x^{0,0}$. This stretching process is coherent and is thus able to generate strong zonal jets u_x^{0,k_y}, which are clearly discernible in the streamlines of the *total* turbulent flow in Fig. 2. The streamlines are colored by their horizontal velocity. Here, *zonal* fluctuations are defined as those fluctuations that do not vary along x (similar to zonal flows in planetary atmospheres [39], where x corresponds to the azimuthal direction). The time scale of zonal-jet generation is significantly longer than the time scale of the KH instability.

Step 4: Jet saturation via coupling to the KH instability

The zonal jets saturate via nonlinear coupling to the turbulent fluctuations in the KH-unstable wavenumber range.

Step 5: Energy cascade to small scales

The KH-scale fluctuations release a fraction of its energy for small-scale cascade. The small scales do *not* drive the large-scale dynamo here.

Step 6: Generation of x-invariant, y-varying vertical fields (b-rolls)

This step is identical to step 2, except that this step applies to magnetic fields instead of flow. The **b**-rolls decay resistively in the absence of nonlinearity. Isomorphic to the **u**-rolls, the **b**-rolls are nonlinearly driven by the KH instability.

Step 7: Generation of mean magnetic field by zonal jets

The **b**-rolls $b_z^{0,-k_y}$ of step 6 are stretched by the phase-locked zonal jets u_x^{0,k_y}, via the field-line stretching term $b_z^{0,-k_y}\partial_z u_x^{0,k_y}$. This process continuously generates the mean field $b_x^{0,0}$, which is reversed in z. Consequently, the gradient of the mean field is continuously steepened. The time scale of the mean-field generation is the longest among all the other steps.

Step 8: Generation of x-invariant, y-varying horizontal fields (zonal fields)

The KH-induced **b**-rolls are stretched by the mean shear flow $u_x^{0,0}$ via the field-line stretching term $b_z^{0,k_y}\partial_z u_x^{0,0}$. This stretching process is coherent and thus generates strong zonal fields b_x^{0,k_y}, which are clearly discernible in the streamlines of the *total* turbulent field in Fig. 2. The streamlines are colored by their strength of the horizontal field, which is the strongest among the three components. The time scale of zonal-field generation is similar to that of zonal-jet generation.

Step 9: Vertical advection of horizontal magnetic fields

The mean horizontal field is advected vertically by the **u**-rolls, thus depleting the mean field and transforming it into a zonal field. Equivalently, this transport of field due to turbulent advection $\langle -\mathbf{u}\cdot\nabla b_x^{0,-k_y}\rangle_{x,y} = -\partial_z(u_z^{0,k_y} b_x^{0,-k_y})$ attempts to flatten the mean-field gradient. In a self-consistent nonlinear regime after kinematic phase, this gradient-flattening transport effect becomes effective—although this effect is found to be generally slightly weaker than the gradient-steepening, field-stretching effect of step 7. Thus, with small remaining nonlinear coupling and resistive dissipation, a quasi-stationary mean field is successfully maintained dynamically.

Step 10: Field saturation via coupling to the KH instability

When horizontal fields — namely, zonal field $b_x^{0,-k_y}$ and mean field $b_x^{0,0}$ — become strong, they resist vertical motions of turbulent flow, thus preventing unphysical growth of magnetic fields without bound. This Lorentz feedback then impacts steps 2 and 6, and thus self-regulates the amplitude of the horizontal fields and induces temporal dynamics in the quasi-stationary oscillatory phase. In this step, energy of the horizontal magnetic fields is also transferred to energy of magnetic fluctuations at the KH-instability scale. Step 10 thus represents the coupling of magnetic fields to the KH instability.

It is to be emphasized that all ten steps of the dynamo cycle do not operate at their full efficiency at the same time. Time delays are inherently introduced by the wide separation of time scales among the very rapid KHI, slowly evolving zonal jets and fields, and yet more slowly evolving mean field. These time lags in linked dynamical systems produce an

inertia that can lead to limit-cycle oscillations [57], which are clearly seen in, for example, time-delay solar dynamo models [58, 59].

IV. NUMERICAL CONFIRMATION OF THE DYNAMO CYCLE

Each step of the dynamo cycle (Fig. 2) is confirmed below using detailed numerical analyses.

Step 1: The KHI

The (x, y)-averaged mean shear flow is KH-unstable, as seen in Fig. 3, where we show the finite-amplitude-modified growth rate $\gamma_{\rm nl}$. The rate $\gamma_{\rm nl}$ — which is mathematically defined in the subsequent paragraph — measures the rate at which energy is transferred from the mean flow to fluctuations during the nonlinear phase. At early times (see the Fig. 3 inset), $\gamma_{\rm nl}$, as found from the initial value solver (direct numerical simulation), agrees with the linear growth rate obtained from the eigenvalue solver.

We define the rate $\gamma_{\rm nl}$ using a straightforward procedure. First, we take the momentum equation

$$\partial_t \mathbf{u}(\mathbf{k}) = L + N, \tag{4}$$

with L and N representing linear and nonlinear operators, respectively. The evolution equation for kinetic energy associated with the wavenumber $\mathbf{k} = (k_x, k_y)$ is then

$$\partial_t \langle |\mathbf{u}(\mathbf{k})|^2 \rangle_z / 2 = \mathrm{Re} \langle \mathbf{u}^*(\mathbf{k}) \cdot L \rangle_z + \mathrm{Re} \langle \mathbf{u}^*(\mathbf{k}) \cdot N \rangle_z, \tag{5}$$

where the angular brackets $\langle \cdot \rangle_z$ represent a z-averaging operation (recall that the mean shear flow is inhomogeneous and non-periodic in z). The first term on the right-hand side of the energy evolution equation is then manipulated to arrive at

$$\partial_t \langle |\mathbf{u}(\mathbf{k})|^2 \rangle_z / 2 = \gamma_{\rm nl} \langle |\mathbf{u}(\mathbf{k})|^2 \rangle_z / 2 + \mathrm{Re} \langle \mathbf{u}^*(\mathbf{k}) \cdot N \rangle_z, \tag{6}$$

where the finite-amplitude-modified growth rate $\gamma_{\rm nl}$ is defined as

$$\gamma_{\rm nl}(\mathbf{k}) = \frac{\mathrm{Re} \langle \mathbf{u}^*(\mathbf{k}) \cdot L(\mathbf{u}(\mathbf{k})) \rangle_z}{\langle |\mathbf{u}(\mathbf{k})|^2 \rangle_z / 2}. \tag{7}$$

In Eq. (7), when $\mathbf{u}(\mathbf{k})$ is replaced with flow fluctuations of the unstable eigenmode at wavenumber $\mathbf{k}$, the rate $\gamma_{\rm nl}$ is exactly the same as the linear growth rate $\gamma_{\rm lin}$ of the KH

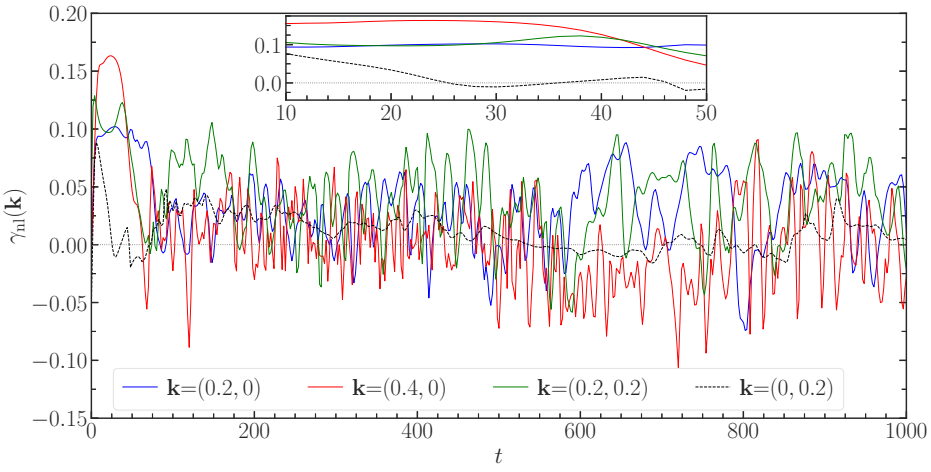

FIG. 3. Finite-amplitude-modified growth rates $\gamma_{\rm nl}$ are obtained by feeding fluctuations with a wavenumber $\mathbf{k} = (k_x, k_y)$ into the linear operator of the flow; see Eq. (7). The rate $\gamma_{\rm nl}$ is constant in time in the early phase of evolution after initial transients have disappeared in the inset. In the nonlinear, quasi-stationary phase, $\gamma_{\rm nl}$ for wavenumbers $k_x{\neq}0$ exhibits fast oscillations. Their time-averaged $\gamma_{\rm nl}$ is larger than the slowly-evolving $\gamma_{\rm nl}$ for $\mathbf{k}$=$(0, 0.2)$. The rate $\gamma_{\rm nl}$ for $\mathbf{k}$=$(0, 0.2)$ is found to be almost entirely due to the fluid advection term (with negligible contribution from the Lorentz force). The parameters used are $M_{\rm A} = 30$, $\tau_{\rm f} = 0.5$, $Re = Rm = 50$, and $\theta = 30\,$deg.

instability at that wavenumber. When flow fluctuations become nonlinear and turbulent, $\gamma_{\rm nl}$ gets modified—in general, the real part of $\gamma_{\rm nl}$ is smaller than $\gamma_{\rm lin}$. The decrement can be dramatic, ranging from a few tens of percent to as much as 99%, depending on the properties of turbulent fluctuations [35, 50].

The smaller $\gamma_{\rm nl}$ for $\mathbf{k} = (0, 0.2)$ explains why zonal jets u_x, whose $\gamma_{\rm lin}$ is zero, take a long time to evolve, compared to the very rapid KH instability (see Fig. 3). Although slowly evolving, the zonal jets carry a significant fraction of turbulent energy, as seen in Fig. 4 (see the solid blue curve).

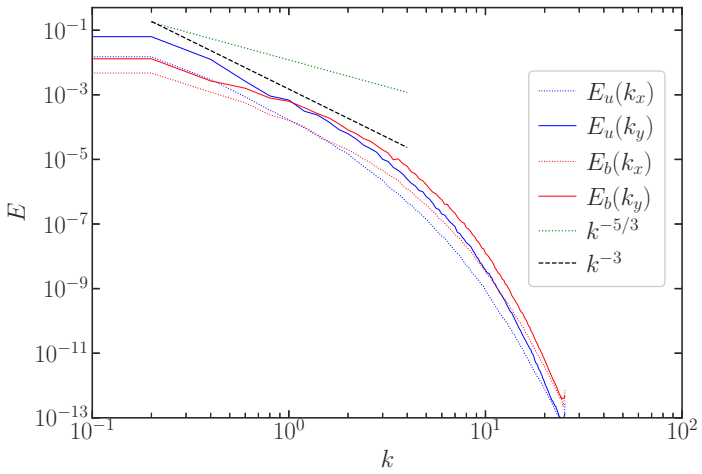

FIG. 4. Typical time-averaged spectra of kinetic energy ($|\hat{\mathbf{u}}(k)|^2/2$) and magnetic energy ($|\hat{\mathbf{b}}(k)|^2/2$) in the saturated stage. Since both spectra are highly anisotropic, the spectra are separately shown as functions of the streamwise wavenumber $k = k_x$ ($k_y = 0$) and spanwise wavenumber $k = k_y$ ($k_x = 0$). Energies are integrated along the non-periodic z-axis. Energies dominantly reside in the harmonics $k_x = 0$.

Step 2: Generation of the x-invariant, y-varying, vertical flows (u-rolls)

The **u**-rolls u_z^{0,k_y} with $k_y \neq 0$ are a seed for the formation of the zonal jets u_x^{0,k_y}. Here, we first analyze what nonlinear mechanism generates the **u**-rolls.

The mean flow and the mean fields do not have vertical components ($\nabla \cdot \mathbf{B} = \partial_z B_z = 0$ for the (x, y)-averaged mean field, and $B_z = 0$ is taken due to the perfectly conducting walls). Moreover, there is no KH instability for $k_x = 0$, meaning that vertical motions of the KH instability do not exist for fluctuations with $k_x = 0$. Thus, the **u**-rolls u_z^{0,k_y} with $k_x = 0$ must be generated purely by nonlinear interactions. Via the nonlinearity, energy is transferred to (from) u_z^{0,k_y} with a wavenumber $\mathbf{k} = (0, k_y \neq 0)$ from (to) a vertical fluctuation with a wavenumber $\mathbf{k}''$ if the energy transfer rate

$$T(u_z^{\mathbf{k}}; \mathbf{k}'') = \mathrm{Re}\left\langle u_z^{-\mathbf{k}} \left(-\mathbf{u}' \cdot \nabla u_z'' + \mathbf{b}' \cdot \nabla b_z''\right)\right\rangle_z , \tag{8}$$

is positive (negative). In Eq. (8), fluctuations with single and double primes are evaluated

at wavenumber $\mathbf{k}'$ and $\mathbf{k}''$, respectively, where $\mathbf{k}' = \mathbf{k} - \mathbf{k}''$.

The top panel of Fig. 5 shows that $T(u_z^{\mathbf{k}}; \mathbf{k}'')$ is predominantly positive at low wavenumbers, indicating that u_z^{0,k_y} is generated by energy transfer from large-scale fluctuations. Small scales act as an energy sink—as expected.

To quantify the relative importance of different turbulent scales, we sum the absolute value of $T(u_z^{\mathbf{k}}; \mathbf{k}'')$ over different scales $\mathbf{k}''$ and normalize this sum to unity. As shown in the bottom panel of Fig. 5, this procedure reveals that 81% of the energy transfer occurs in the range $0 < |\mathbf{k}''| \leq 1$ where the KH instability resides; 11% occurs in the remaining large-scale fluctuations $1 < |\mathbf{k}''| \leq 2$; and merely 8% occurs at small scales $|\mathbf{k}''| > 2$. Thus, Fig. 5 (bottom) confirms that the generation of the **u**-rolls is due to the KH-scale fluctuations.

Step 3: Generation of the x-invariant, y-varying horizontal flows (zonal jets)

To understand the generation of zonal jets, we analyze its energy evolution equation

$$\partial_t \left\langle |u_x^{0,k_y}|^2 \right\rangle_z /2 - \epsilon_\nu = T(u_x^{\mathbf{k}}; \mathbf{k}''), \tag{9}$$

where ϵ_ν is the viscous dissipation rate of large-scale zonal jets and

$$T(u_x^{\mathbf{k}}; \mathbf{k}'') = T_{\rm Adv}(u_x^{\mathbf{k}}; \mathbf{k}'') + T_{\rm Lor}(u_x^{\mathbf{k}}; \mathbf{k}''), \tag{10}$$

with energy transfer via the hydrodynamic advective term given by

$$T_{\rm Adv}(u_x^{\mathbf{k}}; \mathbf{k}'') = {\rm Re}\left\langle u_x^{-\mathbf{k}} \left(-\mathbf{u}' \cdot \nabla u_x''\right) \right\rangle_z , \tag{11}$$

and the energy transfer via the Lorentz force given by

$$T_{\rm Lor}(u_x^{\mathbf{k}}; \mathbf{k}'') = {\rm Re}\left\langle u_x^{-\mathbf{k}} \left(-\mathbf{b}' \cdot \nabla b_x''\right) \right\rangle_z . \tag{12}$$

The spectrum of hydrodynamic energy transfer rate $T_{\rm Adv}(u_x^{\mathbf{k}}; \mathbf{k}'')$ is shown in the top panel of Fig. 6, whereas its bottom panel shows the spectrum of total energy transfer $T(u_x^{\mathbf{k}}; \mathbf{k}'') = T_{\rm Adv}(u_x^{\mathbf{k}}; \mathbf{k}'') + T_{\rm Lor}(u_x^{\mathbf{k}}; \mathbf{k}'')$. Energy is transferred to (from) zonal jets u_x^{0,k_y} with wavenumber $\mathbf{k} = (0, k_y)$ from (to) a fluctuation with wavenumber $\mathbf{k}''$ if the energy transfer rate $T(u_x^{\mathbf{k}}; \mathbf{k}'')$ is positive (negative).

It is a simple exercise to show using Eq. (11) that the advective energy transfer is zero if $\mathbf{k}''$=$\mathbf{k}$ (i.e., $\mathbf{k}'$=$\mathbf{0}$). However, if $\mathbf{k}''$=$\mathbf{0}$ (i.e., $\mathbf{k}'$=$\mathbf{k}$), then energy transfer from the mean shear flow to the jets is non-zero, via the term $-u_z^{0,k_y} \partial_z u_x^{0,0}$

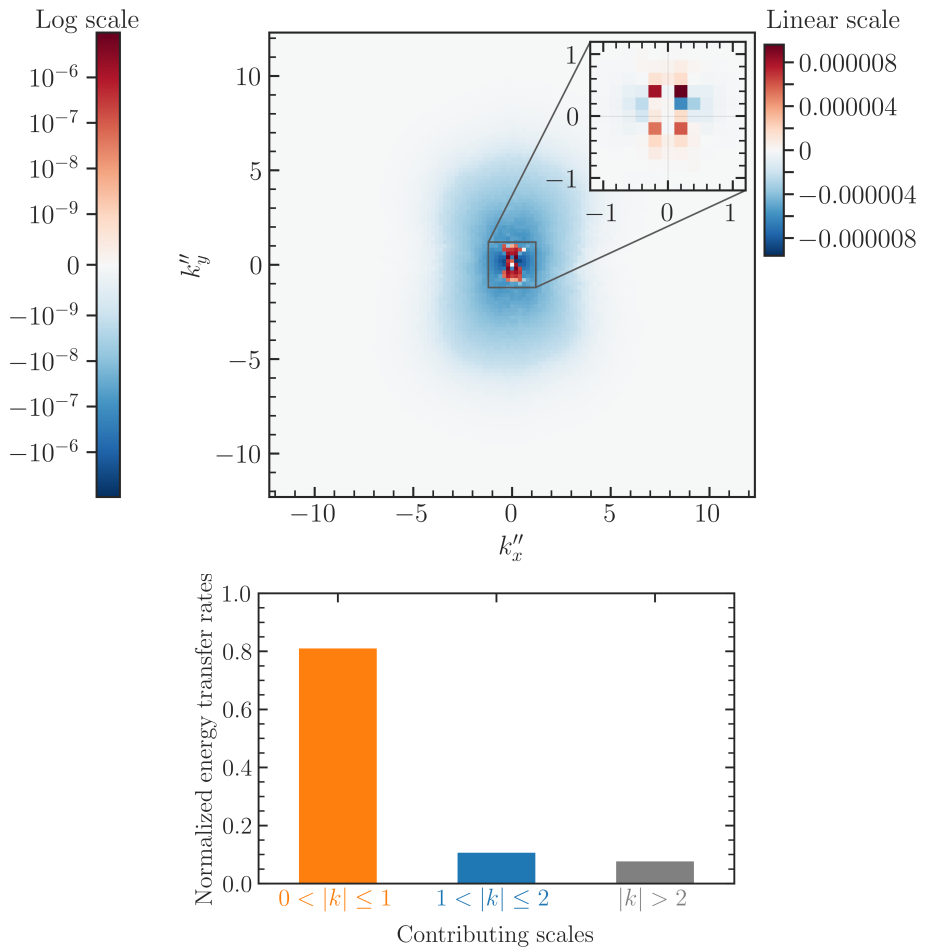

FIG. 5. (Top) Time-averaged rates of energy transfer $T(u_z^{\mathbf{k}}; \mathbf{k}'')$ to u_z^{0,k_y} from various scales $\mathbf{k}''$ via $-\mathbf{u}' \cdot \nabla \mathbf{u}'' + \mathbf{b}' \cdot \nabla \mathbf{b}''$; see Eq. (8). The inset zooms into the central region and highlights the dominant scales with its own color bar using a linear scale, shown on the top right. (Bottom) 81% of the normalized energy transfer is due to the range $0 < |\mathbf{k}''| \leq 1$ where the KH instability resides, 11% is due to the remaining large-scale fluctuations $1 < |\mathbf{k}''| \leq 2$, and merely 8% is due to small scales ($|\mathbf{k}''| > 2$).

We recall that the **u**-rolls u_z^{0,k_y} cannot be generated by the mean flow or the mean fields fields. Thus, the jets are sustained by a *nonlinear* mechanism.

When the **u**-rolls are nonlinearly sustained, the zonal jets receive energy from the mean flow $\mathbf{k}=(0,0)$, via the advective term $-u_z^{0,k_y}\partial_z u_x^{0,0}$. This transfer is shown in the top panel of Fig. 6. This term represents the physical process of coherent straining of the nonlinearly-generated **u**-rolls by the mean shear flow $u_x^{0,0}$. The straining process generates zonal jets u_x^{0,k_y}.

A difference between the straining by a mean shear flow in 3D and in 2D is illustrated in Appendix B.

Step 4: Jet saturation via coupling to the KH instability

The zonal jets saturate by nonlinearly coupling to the turbulent fluctuations in the KH-unstable wavenumber range. This is shown in Fig. 7 where linear and nonlinear energy transfer rates are computed. The linear energy transfer rates are decomposed into multiple contributions: $Q_{u(0,0)}$ is the transfer from the mean flow to the zonal jets; $Q_{b(0,0)}$ is the transfer from the mean field to the zonal jets; and $Q_{\rm ZM}$ is the transfer from the zonal magnetic fields b_x^{0,k_y} to the jets. The nonlinear energy transfer rates are decomposed into $T_{\rm ss}$ and $T_{\rm KH}$. The term $T_{\rm ss}$, when negative, represents the rate of energy transfer from the zonal jets to small scales. The term $T_{\rm KH}$, when negative, represents the rate of energy transfer from the zonal jets to the turbulent fluctuations in the KH-unstable wavenumber range. The large transfer $T_{\rm KH}$ is further decomposed into transfer via the fluid-advective nonlinearity (shown as the blue bar) and transfer via the magnetic nonlinearity (shown as the green bar).

The equation for the evolution of energy $E_{\rm ZF}$ in the zonal jets is

$$\partial_t E_{\rm ZF} = \epsilon_\nu + Q_{u(0,0)} + Q_{b(0,0)} + Q_{\rm ZM} + T_{\rm KH} + T_{\rm ss}, \tag{13}$$

where ϵ_ν is the viscous dissipation of large-scale zonal jets, and the remaining terms are

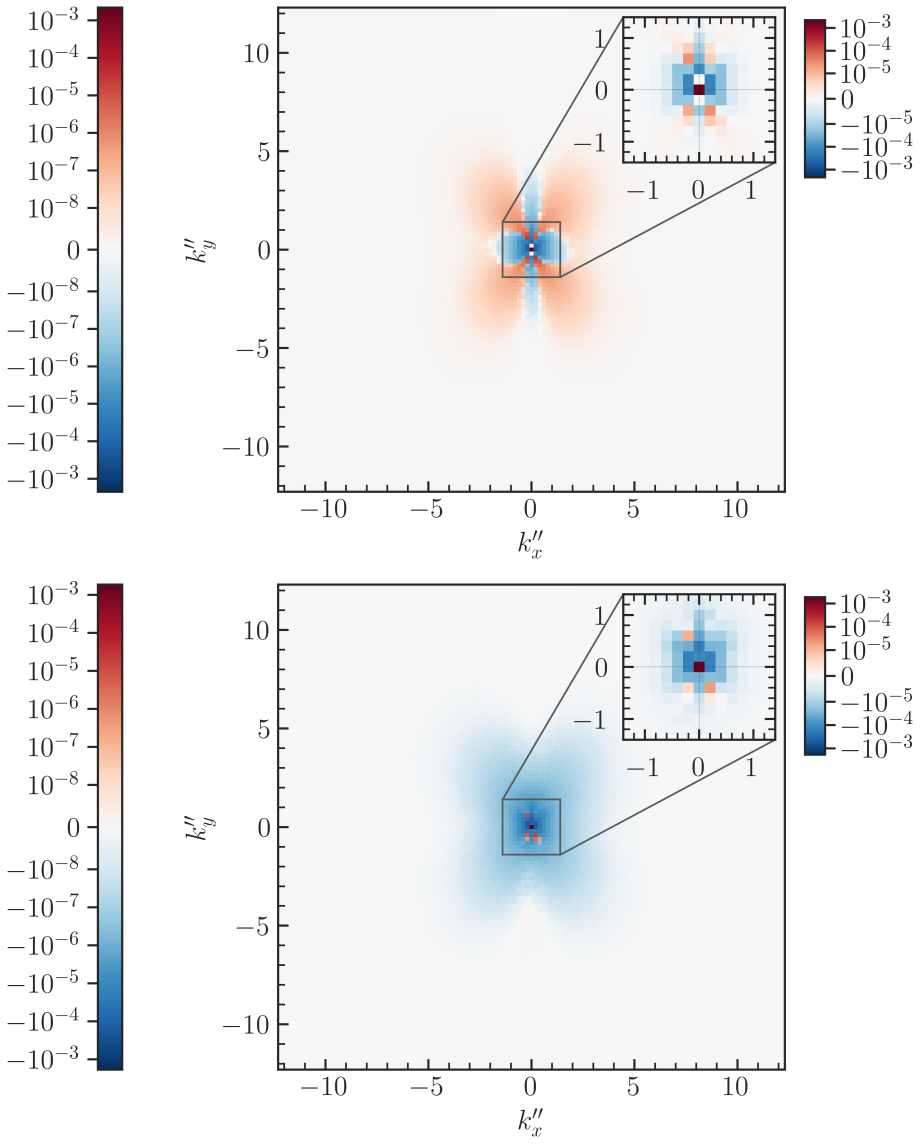

FIG. 6. Time-averaged rates of energy transfer to u_x^{0,k_y} from various scales $\mathbf{k}''$ via hydrodynamic advection $T_{\mathrm{Adv}}(u_x^{\mathbf{k}};\mathbf{k}'')$ (top) and via magnetohydrodynamic interaction $T(u_x^{\mathbf{k}};\mathbf{k}'') = T_{\mathrm{Adv}}(u_x^{\mathbf{k}};\mathbf{k}'')+ T_{\mathrm{Lor}}(u_x^{\mathbf{k}};\mathbf{k}'')$ (bottom). See Eqs. (10)–(12). The insets magnify the central region and highlight the dominant scales with their own color bars, shown on the top right of either panel.

described in the preceding paragraph. These terms are computed using

$$E_{\rm ZF} = \left\langle |u_x^{0,k_y}|^2 \right\rangle_z /2, \tag{14a}$$

$$\epsilon_\nu = \nu \left\langle u_x^{0,-k_y} \nabla^2 u_x^{0,k_y} \right\rangle_z, \tag{14b}$$

$$Q_{u(0,0)} = -\left\langle u_x^{0,-k_y} (\mathbf{u}^{0,k_y} \cdot \nabla u_x^{0,0}) \right\rangle_z, \tag{14c}$$

$$Q_{b(0,0)} = \left\langle u_x^{0,-k_y} (\mathbf{b}^{0,k_y} \cdot \nabla b_x^{0,0}) \right\rangle_z, \tag{14d}$$

$$Q_{\rm ZM} = \left\langle u_x^{0,-k_y} (\mathbf{b}^{0,0} \cdot \nabla b_x^{0,k_y}) \right\rangle_z, \tag{14e}$$

$$T_{\rm KH} = \sum_{\mathbf{k}',\mathbf{k}'' \in \text{ KH-unstable}} \left\langle u_x^{0,-k_y} (-\mathbf{u}' \cdot \nabla u_x'' + \mathbf{b}' \cdot \nabla b_x'') \right\rangle_z, \tag{14f}$$

$$T_{\rm ss} = \sum_{\mathbf{k}',\mathbf{k}'' \in \text{ small scales}} \left\langle u_x^{0,-k_y} (-\mathbf{u}' \cdot \nabla u_x'' + \mathbf{b}' \cdot \nabla b_x'') \right\rangle_z. \tag{14g}$$

Here, $T_{\rm ss}$ captures the nonlinear transfer of energy through scales that are not captured by the other terms of Eq. (13).

Jet saturation is shown in the dynamo cycle as Step 4.

Step 5: Small-scale energy cascade

The free energy from the mean shear flow is tapped by the KH instability, and a fraction of the KH instability energy is released to small scales. The forward energy cascade has recently been quantified in the context of KH turbulence [21].

Step 6: Generation of x-invariant, y-varying vertical fields (b-rolls)

The **b**-rolls b_z^{0,k_y} are a seed for the formation of zonal magnetic fields b_x^{0,k_y}. Here, we analyze what nonlinear mechanism generates the **b**-rolls.

Since the mean flow and mean fields do not have vertical components and since the k_x=0 perturbations have no KH instability, the fluctuation b_z^{0,k_y} is generated purely by nonlinear interactions. Via the nonlinearity, energy is transferred to (from) the **b**-rolls b_z^{0,k_y} with a wavenumber $\mathbf{k} = (0, k_y \neq 0)$ from (to) a vertical fluctuation with wavenumber $\mathbf{k}''$, if the energy transfer rate

$$T(b_z^{\mathbf{k}}; \mathbf{k}'') = \mathrm{Re} \left\langle b_z^{-\mathbf{k}} (-\mathbf{u}' \cdot \nabla b_z'' + \mathbf{b}' \cdot \nabla u_z'') \right\rangle_z, \tag{15}$$

is positive (negative). The spectrum of $T(b_z^{\mathbf{k}}; \mathbf{k}'')$ is shown in Figure 8.

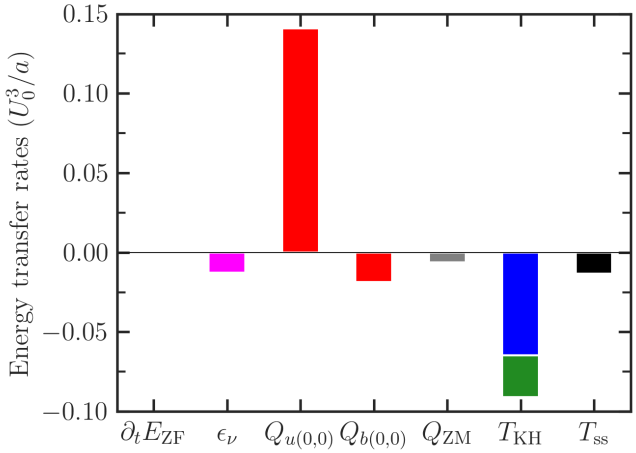

FIG. 7. Zonal-jet energy-transfer mechanisms and saturation balance in a turbulent steady state. The term $\partial_t E_{ZF}$ represents the rate of time-variations of energy of the zonal flow (ZF). This rate of the saturated zonal flow approaches zero upon long time-averaging. The equation $\partial_t E_{\rm ZF} = \epsilon_\nu + Q_{u(0,0)} + Q_{b(0,0)} + Q_{\rm ZM} + T_{\rm KH} + T_{\rm ss}$ represents the energy budget of the zonal flow, where ϵ_ν is the viscous dissipation rate; the other terms represent rates at which the zonal flow receives energy from the mean flow $Q_{u(0,0)}$, the mean field $Q_{b(0,0)}$, the zonal field $Q_{\rm ZM}$, nonlinear fluctuations in the KH-unstable wavenumber range $T_{\rm KH}$, and the remainder of the scales (i.e., small scales) $T_{\rm ss}$. Positive (negative) values of energy transfer rates represent gain (loss) for the zonal flow. The term $T_{\rm KH}$ is further decomposed into flow fluctuations (blue) and field fluctuations (green).

To quantify the relative importance of different turbulent scales, we sum the absolute value of $T(b_z^{\mathbf{k}};\mathbf{k}'')$ over different scales and normalize this sum to unity. This procedure shows that 91% of the energy transfer occurs in the range $0 < |\mathbf{k}''| \leq 1$ where KH instability resides; 6% occurs in the remaining large-scale fluctuations $1 < |\mathbf{k}''| \leq 2$; and barely 3% occurs in small scales $|\mathbf{k}''| > 2$. Thus, Fig. 8 (bottom) confirms that the generation of the **b**-rolls is due to the KH-scale fluctuations.

We have also analyzed the probability density function (PDF) of the fluctuating vertical magnetic fields—a key play player in the dynamo here. The PDFs are centered around zero, as expected, as the mean of the vertical field is zero in the present work. We find, similar to

Seta *et al.* [60], that the PDFs feature non-Gaussian tails in both kinematic and saturated dynamo phases. This analysis further suggests that the vertical magnetic fields are more intermittent in the kinematic stage than in the saturated phase.

Step 7: Generation of mean magnetic field by zonal jets

The mean field in the system we consider cannot be generated directly by the mean flow, because the mean vertical field and the mean vertical flow are both zero ($\nabla \cdot \mathbf{B} = \partial_z B_z = 0$ for the (x, y)-averaged mean field, and $B_z = 0$ is prescribed due to the conducting walls). Therefore, the mean field must be generated entirely by nonlinear interactions. We decompose the nonlinear energy transfer to or from the mean field into three contributions: transfer from large-scale zonal fluctuations is T_{zonal}, corresponding to fluctuations with $k_x = 0$ and $0 < |k_y| \leq 1$; transfer from the KH-scale fluctuations is T_{KH}, corresponding to fluctuations with $0 < |k_x| \leq 1$ and $|k_y| \leq 1$; and transfer from the remainder of the fluctuations T_{residual}, which is obtained from the mean-field energy evolution equation $T_{\text{residual}} = (\partial_t E_b(0,0) - \epsilon_\eta) - (T_{\text{zonal}} + T_{\text{KH}})$. In this expression, $E_b(0,0)$ is the mean-field energy, and ϵ_η is the rate of resistive dissipation of the mean field. A time history of these transfers is presented in Fig. 9(a). The zonal transfer is the largest and almost completely reproduces the total nonlinear energy transfer to the mean field; compare T_{zonal} with $\partial_t E_b(0,0) - \epsilon_\eta$ in Fig. 9(a).

We further decompose T_{zonal} into two elements: zonal-flow stretching $T(\mathbf{b} \cdot \nabla \mathbf{u}_x^{\text{ZF}})$, which transfers energy from the zonal flow (jets) to the mean field; and zonal-magnetic-field advection $T(-\mathbf{u} \cdot \nabla \mathbf{b}_x^{\text{ZM}})$, which transfers energy from the zonal magnetic fields to the mean field. On average, zonal-flow stretching transfers energy to the mean field, and zonal-magnetic-field advection takes energy away from the mean field. These are demonstrated in Fig. 9(b). These effects do not depend on the polarity of the mean field at any given time. Because these two effects occur concurrently and because the field-stretching effect is typically slightly stronger, the mean field takes a longer time to evolve. See Fig. 9(a), where the solid blue curve shows a suitably normalized mean field energy $E_b(0,0)/80$, which evidently evolves slowly (the choice of the proportionality constant, 80, is merely to contain all the curves within the shown y-axis extent, and does not bear any physical meaning).

A simple way to visualize the zonal-flow stretching is to consider the $\mathbf{b}$-rolls $b_z^{0,-k_y}$ that

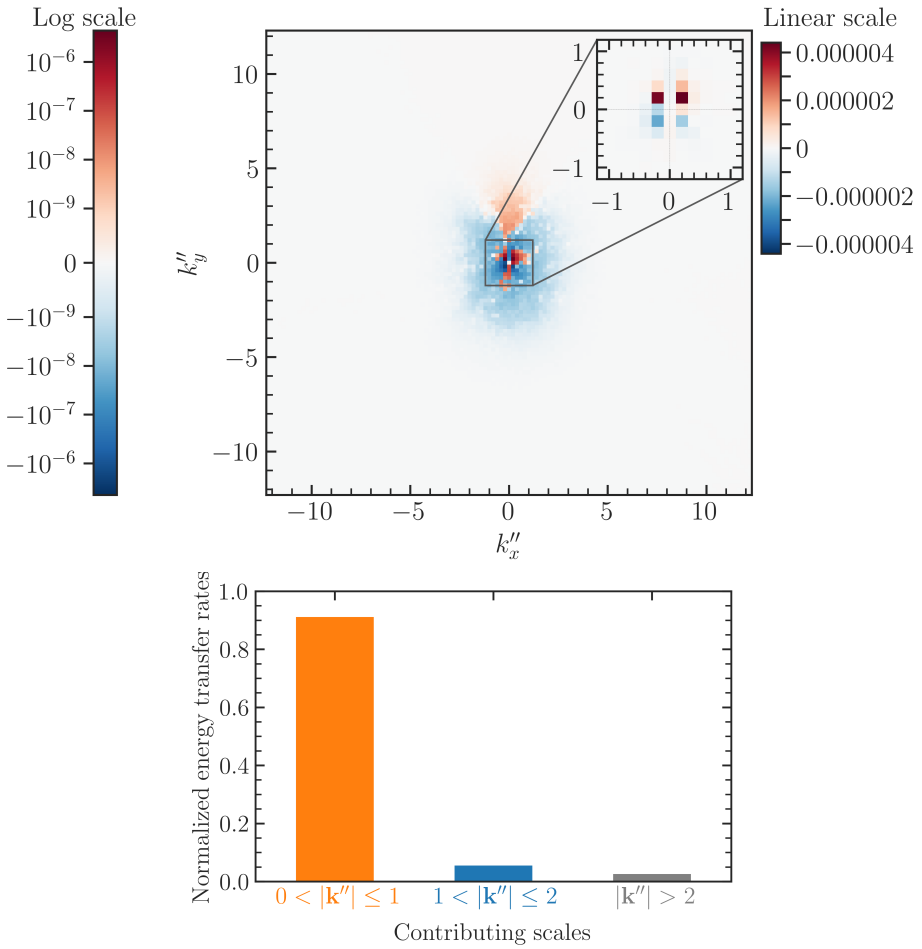

FIG. 8. (Top) Time-averaged rates of energy transfer $T(b_z^{\mathbf{k}}; \mathrm{k}'')$ to b_z^{0,k_y} from various scales $\mathbf{k}''$ via $-\mathbf{u}' \cdot \nabla \mathbf{b}'' + \mathbf{b}' \cdot \nabla \mathbf{u}''$. The inset magnifies the central region and highlights the dominant scales with its own color bar using a linear scale, shown on the top right. (Bottom) 91% of the normalized energy transfer is due to the range $0 < |\mathbf{k}''| \leq 1$ where KH instability resides, 6% is due to $1 < |\mathbf{k}''| \leq 2$, and merely 3% is due to small scales ($|\mathbf{k}''| > 2$).

are strained by the zonal flow u_x^{0,k_y} — not the mean flow $u_x^{0,0}$. This mechanism steepens the mean-field gradient.

The field-line stretching by zonal jets (Step 7) continuously generates the mean field. The zonal jets vary in the y direction and hence do not exist in 2D KH turbulence on the (x, z)-plane. Thus, the dynamo-enabling jets appear only in 3D KH turbulence.

Step 8: Generation of x-invariant, y-varying horizontal fields (zonal fields)

To understand the generation of zonal magnetic fields, we derive the expression for the evolution of energy in zonal magnetic fields

$$\partial_t \left\langle |b_x^{0,k_y}|^2 \right\rangle_z /2 - \epsilon_\eta^{0,k_y} = T(b_x^{\mathbf{k}}; \mathbf{k}''), \tag{16}$$

where ϵ_η^{0,k_y} is the rate of resistive dissipation of large-scale zonal magnetic fields, and $T(b_x^{\mathbf{k}}; \mathbf{k}'')$ is the rate of energy transfer to the zonal magnetic fields from wavenumber $\mathbf{k}''$, which is mathematically given by

$$T(b_x^{\mathbf{k}}; \mathbf{k}'') = \mathrm{Re} \left\langle b_x^{-\mathbf{k}} \left(-\mathbf{u}' \cdot \nabla b_x'' + \mathbf{b}' \cdot \nabla u_x'' \right) \right\rangle_z . \tag{17}$$

The spectrum of $T(b_x^{\mathbf{k}}; \mathbf{k}'')$ is shown in Fig. 10.

To quantify the relative importance of different turbulent scales, we sum the absolute value of $T(b_x^{\mathbf{k}}; \mathbf{k}'')$ over different scales and normalize this sum to unity. This analysis shows that 96% of the energy transfer occurs in the range $0 < |\mathbf{k}''| \leq 1$ where the KH instability resides; 3% occurs in the remaining large-scale fluctuations $1 < |\mathbf{k}''| \leq 2$; and barely 1% occurs at small scales $|\mathbf{k}''| > 2$.

Step 9: Vertical advection of horizontal magnetic fields

The vertical overturning motion of the **u**-rolls generates zonal fields from the mean field. While this mean-to-zonal process can occasionally operate in the reverse direction, the forward process is in general robust and dominant when averaged over a long time. Zonal-magnetic-field advection takes energy away from the mean field. See Fig. 9(b).

To visualize zonal-magnetic-field advection, consider a zonal magnetic field b_x^{0,k_y} that is advected vertically in z by the **u**-rolls u_z^{0,k_y}. Recall that the **u**-rolls vary in y, with their

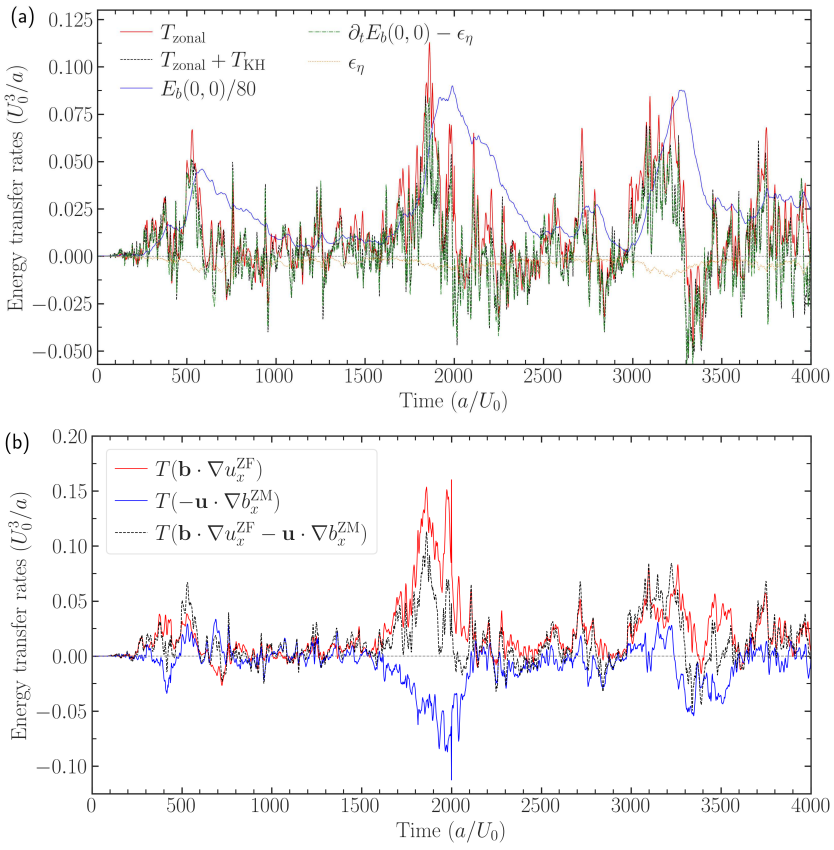

FIG. 9. Rates of energy transfer to and from the mean magnetic field. (a) Energy in the mean field $b_x^{0,0}$ (proportional to the solid blue curve) is shown together with the rates of nonlinear energy transfer to the mean field. The rate at which the mean field receives energy from the zonal ($k_x = 0$) fluctuations is $T_{\rm zonal}$ and that from the Kelvin–Helmholtz instability is $T_{\rm KH}$. The remainder of the nonlinear energy transfer is given by the difference between the dashed-dotted green curve $\partial_t E_b(0,0) - \epsilon_\eta$ and the dashed black curve $T_{\rm zonal} + T_{\rm KH}$. It is found that $T_{\rm zonal}$ contributes $\sim 74\%$ to $T_{\rm zonal} + T_{\rm KH}$; the transfer $T_{\rm KH}$ contributes $\sim 26\%$.

The resistive dissipation of the mean field is ϵ_η. (b) The zonal energy transfer $T_{\rm zonal}$ is further decomposed into the advective and field-line stretching terms: The former (solid blue), on average, takes energy away from the mean field, while the latter (solid red) gives energy to the mean field.

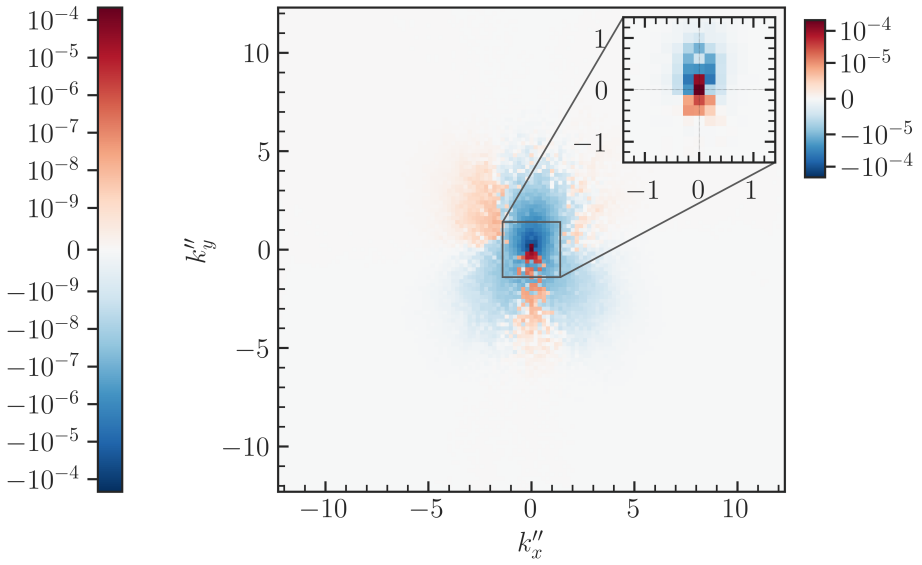

FIG. 10. Time-averaged rates of energy transfer $T(b_x^{\mathbf{k}}; \mathrm{k}'')$ to b_x^{0,k_y} from various scales $\mathbf{k}''$ via $-\mathbf{u}' \cdot \nabla \mathbf{b}'' + \mathbf{b}' \cdot \nabla \mathbf{u}''$. See Eq. (15). 96% of the normalized energy transfer is due to the range $0 < |\mathbf{k}''| \leq 1$ where the KH instability resides, 3% is due to the range $1 < |\mathbf{k}''| \leq 2$, and barely 1% is due to small scales ($|\mathbf{k}''| > 2$). The inset magnifies the central region and highlights the dominant scales with its own color bar, shown on the top right.

vertical motion going up and down at different y-locations. This overturning advective motion reduces the existing mean field (Step 9 in Fig. 2) by converting the mean field into fluctuation fields, namely, the zonal field. This mechanism works to flatten the mean-field gradient, competing with Step 7, and thus counters the rapid steepening of the mean-field gradient.

Step 10: Field saturation via coupling to the KH instability

In the kinematic phase when the mean field grows steadily, we time-average the energy transfer rates to the mean field. See Fig. 11(a). The term $\partial_t E_{b_x(0,0)}$ is non-zero during this growth phase. Zonal fluctuations contribute a majority of the energy transfer T_{zonal} to the

mean field $b_x(0,0)$; the x-direction is the most energetic component of the mean field.

In the saturated dynamo phase ($\partial_t \approx 0$), we time-average the scale-decomposed rates of energy transfer to the mean field. See Fig. 11(b). The large-scale zonal flows (jets with $k_x = 0, 0 < |k_y| \leq 1$) deposit energy $T_{\rm ZF}$ in the mean field. The mean field then saturates by releasing its energy to the large-scale zonal magnetic fields $T_{\rm ZM}$. The remaining energy is released to the KH-scale fluctuations $T_{\rm KH}$. The small-scale transfer $T_{\rm ss}$ is largely decoupled from the mean field.

In this step, the horizontal zonal magnetic fields and mean magnetic fields also have a tendency to inhibit vertical motions associated with the KH instability. This effect is related to the field-line-bending magnetic tension force. To sum up, magnetic fields, when strong, couple back to the KH-scale fluctuations, thus providing a natural mechanism to limit unphysical growth of magnetic fields to unbounded levels. We have found that the turbulent kinetic energy is approximately equal to the mean-flow energy; similarly, the energy in the magnetic fields is approximately equal to the mean-flow energy. This finding of relative levels of energies and mechanisms via which they grow in the kinematic phase will be reported in a forthcoming paper, which details the effect of turbulent stresses and electromotive force and their roles in dynamo action.

V. IMPACT OF THE INITIAL FIELD ON THE DYNAMO

We assess here the impact of the strength and orientation of the initial magnetic field on the dynamo.

A. Presence of an initial externally-imposed mean field

1. *Variation of field strength*

Since the large-scale dynamo involves the KH-scale fluctuations as critical agents, the control parameters that impact the dynamo are anticipated to be parameters that impact the KH instability. We recall that the KH instability is impacted by the presence of an initial externally-imposed mean magnetic field, which introduces a line-bending stabilization effect due to magnetic tension force. When this field is very strong (close to equipartition with the mean flow), the growth rate of the KH instability is substantially reduced. At a critical

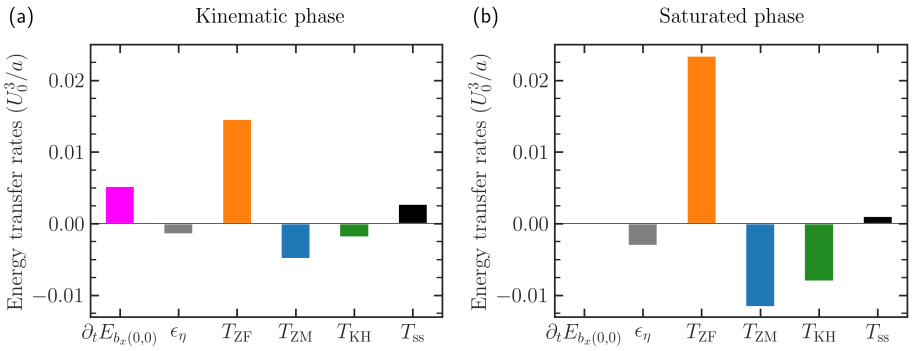

FIG. 11. Time-averaged rates of energy transfer to the mean field during the mean-field growth phase (a) and saturated phase (b). The shown terms satisfy the relation $\partial_t E_{b_x(0,0)} = \epsilon_\eta + T_{\rm ZF} + T_{\rm ZM} + T_{\rm KH} + T_{\rm ss}$, where $T_{\rm ZF}$ is the rate of energy transfer to the mean field from the zonal flow ($k_x = 0, k_y \neq 0$); $T_{\rm ZM}$ is the transfer from the zonal magnetic fields; $T_{\rm KH}$ is the transfer from the KH-scale fluctuations; $T_{\rm ss}$ is the transfer from the remainder of the (small) scales; ϵ_η is the microphysical resistive dissipation of the mean field. Even in the saturated phase, magnetic fields are continuously generated and continuously depleted, thus maintaining a dynamic equilibrium, instead of a static equilibrium.

initial field strength, the growth rate becomes zero. For moderate to weaker fields, the growth-rate reduction is minimal and practically negligible. Since the dynamo is driven by zonal jets stretching the magnetic-field fluctuations (namely, the **b**-rolls), the orientation θ of the initially weak mean field is expected to have a minimal impact on the dynamo. These theoretical expectations are confirmed in Fig. 12. In panels (a)–(c), the root-mean-square amplitudes are shown for the zonal jets $u_x^{0,0.2}$, the **u**-rolls $u_z^{0,0.2}$, and the mean field $b_x^{0,0}$, which all exhibit a similar trend. This trend agrees with the trend of the KH-instability growth rate, which decreases with increasing strength of the initial mean field (i.e., smaller Alfvénic Mach number $M_{\rm A} \propto U_0/B_0$, where B_0 and U_0 are the amplitudes of the mean field and mean flow, respectively).

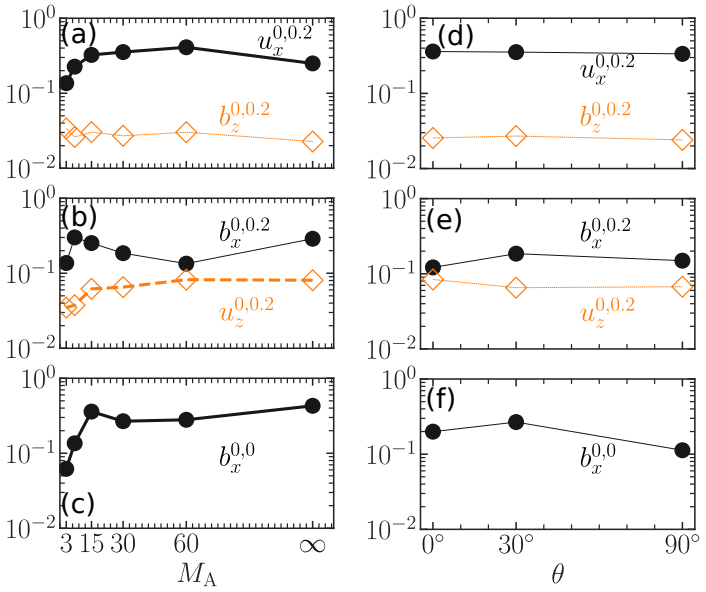

FIG. 12. Impact of initial mean field strength (quantified by the Alfvénic Mach number $M_A \propto U_0/B_0$) and orientation θ on the root-mean-square (rms) amplitudes of different dynamo elements. The case of $M_A^{-1} = 0$ represents the simulation where the initial large-scale magnetic field is zero. The parameter θ measures the angle between the initial mean flow with amplitude U_0 and the initial mean magnetic field with amplitude B_0. The rms amplitude $u_x^{0,0.2}$, for example, is the square root of the energy in the zonal jets, $\sqrt{E(u_x^{0,0.2})}$. The superscript represents the wavenumber (k_x, k_y). (a)–(c) A stronger magnetic field (lower M_A) reduces the growth rate of the KH instability, thus reducing the generation of vertical flow-fluctuations $u_z^{0,0.2}$ in panel (b) and of jets $u_x^{0,0.2}$ in panel (a). The trend of these two elements (shown with thicker lines) is replicated by the mean-field amplitude $b_x^{0,0}$ in panel (c). The absence of an initial large-scale field ($M_A^{-1} = 0$) has no impact on the large-scale dynamo, as the dynamo is driven by the interaction between the fluctuations—primarily between the jets $u_x^{0,0.2}$ and the **b**-rolls $b_z^{0,0.2}$. (d)–(f) Saturated amplitudes of dynamo elements do not depend on the initial-field orientation θ. The minor amplitude variations in panels (d)—(f) are within the statistical variance of the turbulent fluctuations.

2. Variation of field orientation

Dynamo elements are robust to variations in θ, as shown in Fig. 10 (d)–(f). The saturated nonlinear phase is essentially the same for all cases of θ. Minor amplitude variations are within the statistical variance of the turbulent fluctuations.

The case of θ=90° is potentially the most relevant one for the merging of binary neutron stars (BNS), as the magnetic fields in the interface between the BNS when they first come in contact is more likely to be orthogonal to the shear-flow plane. This orientation is expected because the dipolar magnetic fields of each neutron star is orthogonal to the shear-flow plane, located near the equator of the neutron stars The shear-flow plane features the azimuthal flow (directed along ϕ) of the spinning BNS; this azimuthal flow has a strong radial gradient (along r) at the merger interface. The dipolar (axial) magnetic fields of the BNS threads the shear-flow (r, ϕ)-plane that lies between the BNS. Astronomical observations [61, 62] of Gyr-old neutron stars reveal that their total magnetic fields are around 10^8–10^{10} G, corresponding to an energy that is many orders of magnitude lower than that of the mean shear flow in between the BNS approaching to merge [63]. Thus, the initial Alfvénic Mach number for the KH instability at the start of the BNS merger is too large for the KH instability growth rates to be impacted by the presence of this very weak mean field. Instead, the dynamo cycle presented in Fig. 2 generates the magnetic fields via the formation of zonal jets.

B. Absence of an initial mean field

We find that the KH-instability-driven large-scale dynamo operates even in the absence of the initial mean field via the same mechanism described in this article. Using this simulation, the saturated amplitudes of zonal jets, zonal magnetic fields, **u**-rolls, **b**-rolls, and (x, y)-averaged mean magnetic fields are shown in Figs. 12(a)–(c). The case of no guide field ($M_{\rm A}^{-1} = 0$) and the case of a weak guide field are similar in terms of dynamo properties.

VI. DISCUSSIONS ON NONLINEAR SELF-ORGANIZATION

Here we discuss how the self-organization of magnetohydrodynamic 3D KH turbulence differs from or shares similarities with that of hydrodynamic turbulence with local or non-local shear flow. In Sec. VI A, we remark on the differences between the hydrodynamic

and magnetohydrodynamic systems. In Sec. VI B, we offer a general principle of spectral condensation in 3D anisotropic systems; this condensation is different from that observed in isotropic 2D turbulence. Finally, in Sec. VI C, we highlight key differences between turbulence with local and non-local shear flows. The former is readily realized in wall-bounded systems with shear flows (e.g., flows in pipes), whereas the latter is general and excites the KH instability.

A. Comparison of hydrodynamic vs. magnetohydrodynamic 3D KH-instability-driven turbulence

Here, we compare hydrodynamic KH turbulence with magnetohydrodynamic KH turbulence. Steps 1 to 5 of Fig. 2 operate in 3D (magneto)hydrodynamic KH turbulence. Steps 6 to 10 appear only in magnetohydrodynamic turbulence. Steps 6, 8, and 10 are magnetic analogues of the hydrodynamic Steps 2, 3, and 4, respectively.

The zonal jets formed in Step 3 require three dimensions in the system; this process can operate in any general (magneto)hydrodynamic system with a shear flow. Although the zonal jets $u_x(k_x{=}0, k_y{\neq}0)$ are formed when the mean shear flow $u_x(k_x{=}0, k_y{=}0)$ strains the **u**-rolls $u_z(k_x{=}0, k_y{\neq}0)$, the **u**-rolls are generated and sustained by nonlinear interactions. If the nonlinearity is removed in a hydrodynamic system, the **u**-rolls cannot be sustained against viscous dissipation. Recall that the KH instability of the mean flow $u_x(k_x{=}0, k_y{=}0)$ requires fluctuations to have variations along the direction of the mean flow, i.e., $k_x \neq 0$. The fluctuations with $k_x{=}0$ have zero growth rate in the inviscid limit. Since the **u**-rolls have $k_x{=}0$, these rolls require nonlinearity to excite them. The requirement that the **u**-rolls $u_z(k_x{=}0, k_y)$ must couple nonlinearly to the KH-scale fluctuations with $k_x \neq 0$ is evident in

$$\partial_t u_z(k_x{=}0, k_y) = \nu\nabla^2 u_z(k_x{=}0, k_y) - \sum_{\substack{k'_x, k''_x: \\ k'_x + k''_x = 0}} \sum_{\substack{k'_y, k''_y: \\ k'_y + k''_y = k_y}} \mathbf{u}(k'_x, k'_y) \cdot \nabla u_z(k''_x, k''_y) + \dots , \qquad (18)$$

where the ellipsis ... represents the terms irrelevant for the analysis here. These latter terms include, for example, the pressure, which can be recast in terms of the nonlinearity in an incompressible system. Thus, linear physics cannot generate the **u**-rolls.

Similarly, the zonal fields formed in Step 8 require three dimensions in the system; this process can operate in any general magnetohydrodynamic system with a shear flow. Although the zonal fields $b_x(k_x{=}0, k_y{\neq}0)$ are formed when the mean shear flow $u_x(k_x{=}0, k_y{=}0)$

strains the **b**-rolls $b_z(k_x{=}0, k_y{\neq}0)$, the **b**-rolls are generated and sustained by nonlinear interactions. If the nonlinearity is removed in a magnetohydrodynamic system, the **b**-rolls cannot be sustained against resistive dissipation. The requirement that the **b**-rolls $b_z(k_x{=}0, k_y)$ must couple nonlinearly to the KH-scale fluctuations with $k_x \neq 0$ is evident in

$$\partial_t b_z(k_x{=}0, k_y) = \eta\nabla^2 b_z(k_x{=}0, k_y) + \sum_{\substack{k'_x, k''_x: \\ k'_x + k''_x = 0}} \sum_{\substack{k'_y, k''_y: \\ k'_y + k''_y = k_y}} \left[-\mathbf{u}(k'_x, k'_y)\cdot\nabla b_z(k''_x, k''_y) + \mathbf{b}(k'_x, k'_y)\cdot\nabla u_z(k''_x, k''_y)\right]. \tag{19}$$

One may consider a system which features — on top of a mean shear flow $u_x(k_x{=}0, k_y{=}0)$ and a mean field $b_x(k_x{=}0, k_y{=}0)$ — additional components of turbulence-generated flow $u_y(k_x{=}0, k_y{=}0)$ and field $b_y(k_x{=}0, k_y{=}0)$. In our nonlinear simulations, the energies in these components are confirmed to be at least two orders of magnitude smaller than the x-directed mean flow and fields. Even in the more general case, $b_z(k_x{=}0, k_y)$ cannot be perpetually sustained against resistive dissipation *without a nonlinearity*. The **b**-rolls $b_z(k_x{=}0, k_y)$ decay away resistively following a wave-like damped solution. The explanation is straightforward: For sustained dynamo action with the magnetic field $b_z(k_x{=}0, k_y)$ varying in two dimensions (y and z), the flow must vary in all 3 dimensions—a requirement imposed by the anti-dynamo theorems [64, 65]. Hence, there must be nonlinear couplings among the 3D fluctuations. The linear couplings between the mean flow and the x-invariant fluctuations ($k_x{=}0, k_y \neq 0$) alone cannot *sustain* generation of magnetic fields (it is recalled that transient growth of magnetic fields occurs in 2D, as well, where the dynamo does not exist).

The foregoing discussions highlight some comparison between the 3D hydrodynamic and 3D MHD systems. The prominent similarity between the two systems is the existence of robust zonal jets [35].

The jets are the central engine in the operation of the dynamo driven by the mean-vorticity effect [22]. We have performed numerical experiments where we scrambled the phases of the zonal jets (making them incoherent), and we observe that the dynamo is inactive. Since the zonal jets are direct products of the **u**-rolls, we have performed additional experiments where we scrambled the phases of the **u**-rolls, and we find that the zonal jets are not prominent—and thus, there too, the dynamo is inactive. In these experiments, where the system is forced to eliminate the zonal jets, we observe that the turbulence is dominated largely by 2D KH-scale fluctuations throughout the nonlinear phase; the transition from 2D

to 3D motions in our standard setup is severely impacted. This lack of 2D-to-3D transition is simple to explain if one recalls that the zonal jets are efficient channels for coupling 2D and 3D fluctuations. To illustrate further, consider a triad interaction between the three wavenumbers: the zonal jets with a wavenumber $\mathbf{k}$=$(0, k_y)$, the 2D KH instability with $\mathbf{k}$=$(k'_x, 0)$, and the 3D KH instability with $\mathbf{k}$=(k''_x, k''_y), where k''_x= $-$ k_x and k''_y=k_y $-$ k'_y. In this wavenumber triad, if the zonal wavenumber is forcefully suppressed manually, the nonlinear channel that couples the 2D and 3D KH-scale fluctuations is significantly impacted. Thus, the 2D and 3D KH-fluctuations are not able to interact as much. When the 2D KH-scale fluctuations dominate the turbulence, the dynamo is ineffective (by Cowling's [64] and Zeldovich's theorems [65]).

B. Spectral condensation and wave-anisotropy principle in 3D turbulence

Here, we present a general principle of spectral condensation and saturation physics in 3D systems where symmetry is broken, making the system anisotropic.

Due to the presence of an inhomogeneous mean shear flow, the system we consider is anisotropic. Whenever a system is anisotropic, it is expected that large-scale coherent structures will emerge in the nonlinear phase. We refer this expectation as the wave-anisotropy principle. This general principle applies to any system where anisotropy is introduced by an external physics, e.g., rotation, a mean (guide) magnetic field, a large-scale shear flow, stratification, etc. In such an anisotropic system, the linear waves feature an anisotropic spectrum of wave-frequency or growth rate over a wavenumber plane, say $\mathbf{k} = (k_\perp, k_{||})$. Here, $k_{||}$ and $k_\perp$ are defined with respect to the direction of anisotropy arising from the external physics, e.g., rotation, a mean (guide) magnetic field, a large-scale shear flow, stratification, etc.. Because of the anisotropy, the growth rate or frequency of a linear wave is zero or nearly zero along one of the axes, say $k_\perp$. Conversely, along the parallel direction $k_{||}$, the growth rate (frequency) is non-zero and different for different $k_{||}$.

To illustrate, consider Alfvén waves (or Rossby waves), whose frequencies ω in the small-wavenumber limit are proportional to $k_{||}$: $\omega \propto k_{||}$, where $k_{||}$ the component of the wavenumber along the direction parallel to the external magnetic field (or the equatorial direction for Rossby waves in a beta plane). In such a case, there exists a wavenumber $\mathbf{k} = (\mathbf{k}_\perp, k_{||}$=$0)$ that is expected to feature a zero-frequency (or a very-low-frequency) coherent structure.

The nature of this coherent structure can be predicted *a priori*: Consider the nonlinearity, e.g., $\mathbf{u}\cdot\nabla\mathbf{u}$, and examine the property of $\mathbf{u}$ to predict the nature of the coherent structure. The component of the coherent structure $u_{||}(\mathbf{k}_\perp, k_{||}{=}0)$ pointed along the parallel direction reduces the nonlinearity to exactly zero. For the wavenumber $\mathbf{k} = (\mathbf{k}_\perp, k_{||}{=}0)$, the gradient operator becomes $\nabla = i\mathbf{k}_\perp$. That is, $\mathbf{u}\cdot\nabla\mathbf{u} = \mathbf{u}_\perp i\mathbf{k}_\perp(u_{||}\hat{\mathbf{e}}_{||} + \mathbf{u}_\perp\hat{\mathbf{e}}_\perp)$. Thus, if a system has only a coherent structure $u_{||}(k_\perp, k_{||}{=}0)$, no matter how large its amplitude is, the nonlinearity is always exactly zero. Hence, $u_{||}(\mathbf{k}_\perp, k_{||}{=}0)$ is an exact *nonlinear* solution to the ideal equations of motion. This nature is similar to that of the Elsässer fields, which are exact nonlinear solutions to the ideal MHD equations [43]. In a general turbulent system, however, there inevitably exist other kinds of fluctuations $\mathbf{u}(\mathbf{k}_\perp, k_{||} \neq 0)$—although the coherent flow $u_{||}(\mathbf{k}_\perp, k_{||}{=}0)$ tends to dominate over the remainder of the fluctuations. This property explains the origin of jets in the present KH-instability-driven system in 3D, and the origin of jets in the Goldreich–Schubert–Fricke-instability-driven turbulence [66], among others [37, 67–73].

The wave-anisotropy principle applies to a wide variety of systems, such as quasi-geostrophic turbulence, Hasegawa-Wakatani turbulence, Hasegawa-Mima turbulence, rotating 3D turbulence, magnetized 3D turbulence, etc., all of which lead to the formation of large-scale anisotropic, coherent fluctuations [37, 67–73]. Here, the wave-anisotropy principle has been shown to be a key ingredient of the mean-vorticity-driven dynamo [22].

C. Secondary instability vs. primary instability in self-sustaining of jets

Here, we remark on key differences between turbulence with local and non-local shear flows, and measure efficiencies of primary and secondary instabilities.

When a mean shear flow varies linearly along a spatial dimension (say, z), the mean flow is stable to the Kelvin–Helmholtz instability; the instability requires a non-zero second derivative in the flow profile. Considering a mean flow with a linear profile, past studies (see, e.g., Refs. [7, 74, 75]) have shown that straining by the mean shear flow is robust, leading to the formation of zonal jets $u_x(k_x{=}0, k_y \neq 0)$; see Step 3 in Fig. 13(a). However, to sustain the generation of zonal jets, Step 2—a nonlinear mechanism—is required; otherwise, zonal jets are formed only transiently before they decay and disappear completely. If the mean flow $U_x(z)$ lacks an inflection point ($\partial_z^2 U_x = 0$), the primary KH instability of Step 1 cannot

operate. In that case, it has been suggested that the nonlinear zonal jets $U_x(y,z)$—pointing along x and varying sinusoidally along y—may become KH-unstable secondarily, thus generating fluctuations that vary in all three dimensions. This process of jets feeding back on jets is sometimes called the self-sustaining jet-formation mechanism (SSJFM) in studies of wall-bounded shear flow $U_x(z)$ that is linearly stable to the KH instability [74].

Based on the consideration in the foregoing paragraph [74] which is limited to a KH-stable mean flow (e.g., a linear shear flow), it has been speculated that the same SSJFM holds true for an arbitrary shear flow. However, this speculation ignores an important reality: If the mean shear flow has a non-zero second derivative (flow curvature), the mean flow can itself drive a primary instability that can rapidly generate 3D fluctuations. See Step 1 in Fig. 13(a). This primary mechanism can easily dominate over any secondary SSJFM.

To test the efficiencies of the primary and secondary instabilities in their ability to generate 3D fluctuations, we compare the energy transfer rates to 3D fluctuations from the mean flow (see Fig. 13(b)) against that from the zonal jets (see Fig. 13(c)), using Eq. (20). The former is found to be an order-of-magnitude larger than the latter. This finding demonstrates that the primary KH instability of the mean shear flow generates 3D fluctuations overwhelmingly: The secondary KH instability of the zonal jets generates 3D fluctuations at a rate that is insignificant.

The primary mechanism operates even in the absence of a nonlinearity, whereas the secondary mechanism can only become active in the nonlinear phase. The rates of energy transfer via primary and secondary mechanisms are computed using

$$\begin{aligned}\partial_t\langle \mathbf{u}_i(-\mathbf{k})\mathbf{u}_i(\mathbf{k})\rangle_z = &\underbrace{-2\mathrm{Re}\langle u_i(-\mathbf{k})u_j(\mathbf{k})\partial_j u_i(0,0) + u_i(-\mathbf{k})u_j(0,0)\partial_j u_i(\mathbf{k})\rangle_z}_{\text{KH of mean flow (primary instability)}} + \\ &\underbrace{-2\mathrm{Re}\langle u_i(-\mathbf{k})u_j(\mathbf{k}')\partial_j u_i(0,k_y) + u_i(-\mathbf{k})u_j(0,k_y)\partial_j u_i(\mathbf{k}')\rangle_z}_{\text{KH of zonal jets (secondary instability)}} + ...,\end{aligned} \tag{20}$$

where the ellipsis ... represents the terms not relevant for discussion here. The first term on the right-hand side of Eq. (20) measures the rate of energy transfer to the fluctuation with wavenumber $\mathbf{k}$ from the mean flow $u_i(0,0)$. This energy transfer rate can be converted into the growth rate by dividing the first term on the right-hand with the energy $\langle \mathbf{u}_i(-\mathbf{k})\mathbf{u}_i(\mathbf{k})\rangle_z$; this growth rate corresponds to the finite-amplitude-modified growth rate of the KH instability of the mean shear flow in the nonlinear phase (see Fig. 3). The second term on the right-hand side of Eq. (20) measures the rate of energy transfer to fluctuations

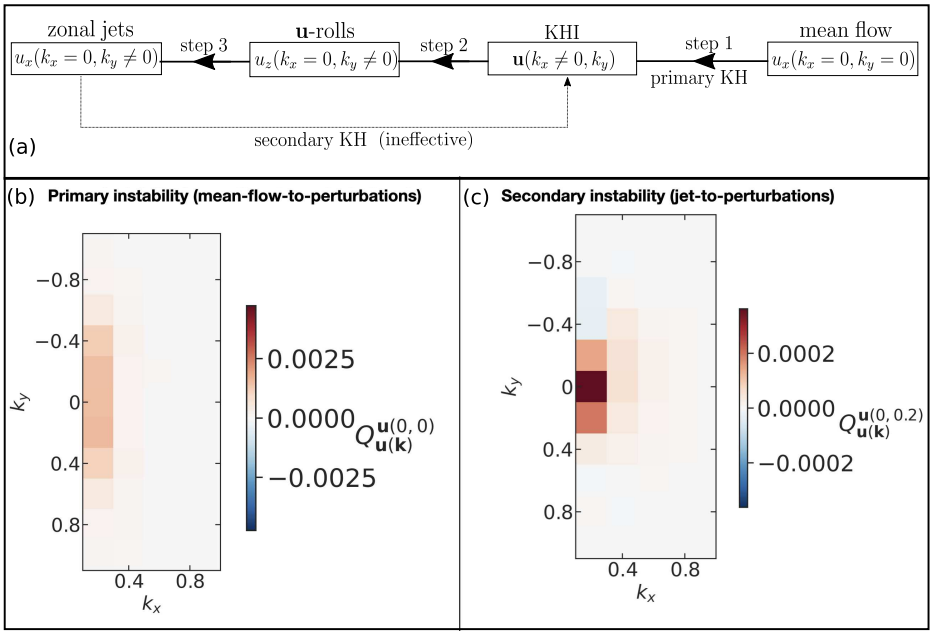

FIG. 13. The primary instability of the mean shear flow dominates over the secondary instability of the zonal jets by supplying an order of magnitude more energy to 3D KH-unstable fluctuations. (a) Step 1 represents the primary KH instability of the mean flow; Step 2 represents a nonlinear mechanism, namely, the advective nonlinearity $-(\mathbf{u}\cdot\nabla)\mathbf{u}$; Step 3 represents straining by the mean flow. These three steps are described in Fig. 2 with the same numbering convention. If the mean shear flow $u_x(k_x{=}0, k_y{=}0)$ does not undergo the KH instability, Step 1 is absent. Panels (b) and (c) show the rates of energy transfer to different wavenumbers $\mathbf{u}(\mathbf{k})$ from the mean shear flow and from the zonal jets, respectively. As these data show, the understanding based on KH-stable linear shear flow is inapplicable when the turbulence is driven by a KH-unstable flow. Specifically, turbulence with a KH-*stable* mean shear-flow operates via a less-energetic secondary instability (i.e., the mechanism where the KH instability of zonal jets generates 3D fluctuations, namely those with $k_x \neq 0$; these 3D fluctuations are required to power zonal jets). However, turbulence with a KH-*unstable* mean shear-flow operates via a more-energetic primary instability (i.e., the mechanism where the KH instability of the mean shear flow directly generates 3D fluctuations, thus sustaining the generation of strong zonal jets).

with wavenumber $\mathbf{k}$ from the zonal jets $u_i(0, k_y)$. The second term of Eq. (20) is an order of magnitude smaller that the first term.

VII. CONCLUSIONS

This work has unveiled an essential nonlinear network of dynamic interactions between flow and magnetic fields in a dynamo cycle driven by the Kelvin–Helmholtz (KH) instability of a maintained mean shear flow. The network detailed in Fig. 2 explains a recent and novel finding that the profile of (x, y)-averaged mean magnetic field generated by the KH instability is nearly identical to that of the (x, y)-averaged mean shear flow. This phenomenon arises even in the absence of the initial mean magnetic field. It is noted that the mean field $B_x(z)$ and the mean flow $U_x(z)$ do not directly couple, i.e., the field-line stretching term $\mathbf{B} \cdot \nabla_z U_x(z)$ is zero. This fact is due to the absence of the mean vertical field B_z in the direction z: $\nabla \cdot \mathbf{B} = \partial_z B_z = 0$ for the (x, y)-averaged mean field, and B_z is zero for perfectly conducting boundaries. Thus, the mean horizontal field is generated by a sequence of nonlinear interactions among fluctuations. Using nonlinear energy transfer analyses, this work has shown that the mean field and the mean flow are linked by 4 steps in a chain of magnetohydrodynamic interactions: In the first step, the mean shear flow $U_x(z)$ linearly excites the 2D and 3D KH instability fluctuations, which have $k_x \neq 0$. In the second step, KH-unstable fluctuations nonlinearly generate x-invariant, y-varying vertical flow (fields), which are labeled **u**-rolls (**b**-rolls), borrowing nomenclature from the studies of wall-bounded, KH-*stable* shear flows. In the third step, the **u**-rolls (**b**-rolls) are strained by the mean horizontal shear flow $U_x(z)$, thus transforming the rolls into x-invariant, y-varying horizontal flows (fields), labeled zonal jets (zonal fields). Hence, the jets acquire a vertical profile similar to the gradient of the horizontal mean flow $\nabla U_x(z)$. The sustained generation of the jets requires nonlinear KH instability motions varying in all three dimensions. (The foregoing three steps are hydrodynamic in nature.) In the final step, the zonal jets stretch the **b**-rolls, thus creating mean magnetic fields. Since this field-line-stretching process involves the spatial gradient of the jets, the mean magnetic fields display a spatial profile similar to the second derivative of the mean shear flow $\nabla^2 U_x(z)$—the first derivative arises in the jet-creation process, the second in the mean-field creation process.

Additional steps of the dynamo cycle relate to the saturation of the mean fields. The

spatial gradient of the mean field is steepened by the shear-flow-induced jets (Step 7 in Fig. 2). The steepened mean-field gradient is flattened by turbulent advection of mean fields along the direction of mean-field gradient (step 9 in Fig. 2). This flattening is similar to the turbulent advection of the mean momentum that flattens the mean shear layer. When the mean fields are advected (overturned) by the **u**-rolls vertically, the mean fields get depleted, as the mean fields transform into zonal magnetic fields. Zonal fields are additionally generated (Step 8 in Fig. 2) when the mean shear flow strains the **b**-rolls. These **b**-rolls are created by the KH instability (Step 6 in Fig. 2). Zonal fields, when strong, tend to inhibit vertical KH instability motion, thus arresting the unbounded growth of the magnetic fields and leading to saturation (Step 10 in Fig. 2). These various steps operate on their own characteristic timescales—very rapid KH instability, slow zonal jets and zonal fields, and even slower mean field. This separation of time scales naturally endows the dynamo cycle with inertia, self-organization, and the tendency for cyclic behavior, which is consistent with the observed astrophysical magnetic fields.

Inherently three-dimensional zonal jets develop as a spectral condensate. This condensate is sustained by the KH instability. The instability is found to not directly generate mean field but rather act as a crucial enabler of the dynamo. The KH instability of the mean shear flow sustains the nonlinear generation of the **u**-rolls, which are then strained by the mean shear flow to produce the zonal jets. These jets then create the mean field. The jets are exact nonlinear solutions to the 3D magnetohydrodynamic equations, hence they are resilient to occasional large-amplitude perturbations. Additionally, because the jets are directed along the x axis and do not vary along the x axis, the x-gradients of the fluid pressure and the magnetic pressure are exactly zero, thus leading to minimal impact of the Lorentz feedback on the jets. This topological protection of the jets against strong Lorentz feedback makes the jets robust. The jets are the central engine of the dynamo cycle uncovered in this work.

The jets are robust to variations in key magnetohydrodynamic parameters such as the strength of the initial mean magnetic field superimposed on the KH instability. The orientation of the initial mean field has no impact on the nonlinear saturation properties of the dynamo. The jet-driven dynamo operates even in the absence of the initial mean field, so long as the unstable mean flow is maintained to sustain the interactions of the dynamo. The maintenance of the mean flow is required because the mean-field creation takes a longer time, while the mean shear flow—if not maintained—can quickly deplete due to the mo-

mentum transport driven by the fast KH instability. The essential steps of the dynamo cycle are driven primarily by the large-scale fluctuations ($|k|a \lesssim 2$, where k is the horizontal wavenumber and a is the half-width of the shear layer). Smaller physical scales ($|k|a \gtrsim 2$) contribute only 1% to 10% to the energy transfer to zonal jets, zonal fields, and mean field, among others. This finding confirms that, in the large-scale dynamo here, energy-containing large-scale eddies are the dynamo source; and the inertial-range eddies merely act as a dynamo sink to dissipate small amount of energy. This reasoning explains why the large-scale dynamo was found to be robust to variations in the small-scale visco-resistive properties [21].

This work focuses on the KH-instability-driven turbulence and the subsequent dynamo processes. Since the large-scale KH instability nonlinearly couples to all scales, including the small scales, and thus naturally stirs those scales, this work does not require an additional external stirring; the latter is required in homogeneous, isotropic turbulence. In many dynamo studies [46, 76], especially those using a KH-stable shear flow, one is required to externally stir turbulent motions; otherwise, in the absence of turbulence, there is no dynamo. However, here, the KH instability—arising from a nonlocal, unstable shear flow—naturally stirs all scales, and self-consistently controls the properties of turbulence. We emphasize that the distinction between *strong* and *weak* shear-flow does not exist in the current problem, because the dynamo here does not require an additional artificial external stirring f_t, and the relative importance of shear and f_t is, therefore, moot. Here, we have only two cases: either there is an unstable shear flow ($U_0 \neq 0$), or there is no unstable shear flow ($U_0 = 0$). In the presence of an unstable shear flow, the dynamo exists, provided that the viscosity and resistivity are not enormously large, suppressing the KH instability and damping out the entire fluctuation spectrum. In the absence of an unstable shear flow in this work, there is no dynamo, as there is no turbulence.

The role of cross-helicity in dynamos with the mean-vorticity-effect [22] is apparent if one compares the flow and magnetic fields in Fig. 2. For example, comparing the mean flow and the mean magnetic field, we note that they are similar except that the red (positive) of one is blue (negative) of another and vice-versa, i.e., the flow and fields are anti-aligned at the shown time. This anti-symmetry is prominent when one compares **u**-rolls with **b**-rolls and when one compares zonal jets with zonal fields. The flows and fields at large scales are anti-symmetric at the shown time. Over a longer time, the flows and fields become

symmetric and then anti-symmetric and so on. Thus, cross-helicity plays a critical role in the dynamo with a driven shear flow.

The dynamo cycle helps inform sub-grid models of dynamo and turbulence [77–79], which can be implemented in resolution-limited global simulations of general-relativistic binary neutron star mergers [63, 80]. In these mergers, the KH instability is expected to generate ultra-strong magnetic fields [11], possibly stronger than magnetar fields. The present dynamo cycle also identifies a working mechanism behind a postulated non-traditional mean-field dynamo theory—the mean-vorticity effect [22]. This mean field theory is a simple coarse-grained description of the complex turbulent process detailed in this work. The KH dynamo life-cycle we describe here is likely present in non-kinematic simulations of MHD turbulence in the presence of a sinusoidal shear flow [81, 82]; sinusoidal shear flows are KH-unstable [83]. As this current work suggests, many astrophysical dynamos are likely driven by hydrodynamically unstable shear flows, which display large-scale vorticity [84] and form jets.

ACKNOWLEDGMENTS

We thank the anonymous reviewers for helpful comments that strengthened the presentation of the work. For fruitful discussions, it is our pleasure to thank D. Lecoanet, J.R. Beattie, A. Bhattacharjee, A.M. Beloborodov, K.J. Burns, and J.S. Oishi. This material is based upon work funded by the National Science Foundation (NSF) under award 2409206 and Department of Energy (Grant No. DE-SC0022257) through the DOE/NSF Partnership in Basic Plasma Science and Engineering. A.E.F. is supported by an NSF Astronomy and Astrophysics Postdoctoral Fellowship under award AST-2402142. This work used Anvil at Purdue University through allocation TG-PHY130027 from the Advanced Cyberinfrastructure Coordination Ecosystem: Services & Support (ACCESS) program. Staff support from Anvil and additional computing resources from Bridges-2 are gratefully acknowledged.

APPENDIX A: DISCUSSION ON THE MAINTENANCE OF THE LARGE-SCALE SHEAR FLOW

Large-scale shear flows are ubiquitous in astrophysics as they are driven by various forces such as gravity and thermodynamics operating from stars to galaxies. To model these diverse and complex situations, we take a simple approach where we isolate the main physics of shear, because we are interested in understanding the fundamental role of non-uniform shear in the dynamo. We present below discussions on the choice of the large-scale-flow forcing and the physics behind it.

1. Our objective in this paper is to maintain a large-scale shear flow, so that the shear flow remains unstable and drives turbulence at all times, thus avoiding the decaying turbulence. We are interested in understanding the role of non-uniform large-scale shear in the dynamo. We find that the dynamo emerges in both cases that we have simulated: (i) the large-scale shear flow is allowed to evolve in time and driven back to its initial unstable equilibrium; and (ii) the large-scale shear flow is frozen, making it static in time. These experiments demonstrate that, as long as the large-scale shear flow is replenished, the dynamo operates in essentially the same way, regardless of how the shear is replenished.

2. Next, we provide a mathematical justification for the simple "Krook drive," routinely used in plasma physics [33, 83] and fluid dynamics [30]. We note that the (Krook) forcing function $f(\langle u_x(t{=}0)\rangle_{x,y} - \langle u_x(t)\rangle_{x,y})$ drives the flow back to its initial, unstable, reference profile $\langle u_x(t=0)\rangle_{x,y}$. Such functional form of forcing has also been used in the context of fusion plasmas and magnetic reconnection [33]. Note that the forcing function f here is an external acceleration, measured in units of U_0^2/a, where U_0 is the amplitude of the mean flow with shear-layer half-width a. We write a general expression $f = \frac{U_0^2}{a} \times g\,(\epsilon)$, where $g\,(\epsilon)$ is an arbitrary function of the non-dimensional ϵ, given by $\epsilon = aU_0^{-2}\tau_{\rm f}^{-1}\left[\langle u_x(t{=}0)\rangle_{x,y} - \langle u_x(t)\rangle_{x,y}\right]$. Considering small deviation ϵ, we take $g\,(\epsilon) = \epsilon$ because this is a commonly used form and because it represents a regime of "soft" forcing described in the next point immediately below.

3. If one were to consider nonlinear dependence on ϵ in the forcing function (mentioned in the preceding point), the large-scale flow would be more aggressively forced toward

the initial reference flow. In this work, we focus on "soft" forcing that is linear in ϵ, ensuring that the flow spans a broader range of temporal fluctuations. We emphasize that, even for the case of $\tau_{\rm f} = 0$, i.e., a frozen (time-static) large-scale flow, our simulation confirms that the dynamo life-cycle is essentially the same; hence, it is expected that even with other nonlinear forms of the forcing, the same dynamo life-cycle emerges. The key in obtaining the dynamo life-cycle is not necessarily *how* the large-scale flow is replenished, but *whether* the large-scale flow is replenished.

4. The forcing used in this work is motivated by both mathematical and physical arguments mentioned above. The parameter $\tau_{\rm f}$ is not arbitrary but is to be compared to the physics of the instability considered in this work. In distinct simulations, we have varied $\tau_{\rm f}$, and by extension varied the nature of the forcing. Over a broad range of $\tau_{\rm f}$, we have found similar dynamo properties. We conclude that, as long as the forcing timescale $\tau_{\rm f}$ is shorter than the instability-growth time, the kinetic energy in the large-scale flow is always replenished faster than the rate at which the instability extracts energy from the large-scale shear. The maintained shear-flow then leads to the dynamo life-cycle reported in this paper.

The above considerations thus provide necessary physical and mathematical justifications for the choice of the forcing and the physics behind it.

APPENDIX B: RAPID DISTORTION THEORY IN 2D VS. 3D: EDDY SPLITTING VS. EDDY STRENGTHENING

Shear flows can distort eddies and split them apart across the axis of the flow-gradient [28]. This eddy splitting, or scale shortening, applies to all 2D and 3D perturbations, except one particular class of perturbations that are topologically protected. This class of perturbations have a topology such that they do not vary along the direction of the mean shear flow.

For the eddy-splitting or scale-shortening to apply, the perturbations must vary along the direction of the mean flow. This result is easily understood if one considers a simple linear shear flow (which may be thought as zooming into the hyperbolic tangent shear layer where the mean flow is close to zero, so the leading-order term is linear in the spatial coordinate, thus making the rapid distortion theory applicable [26]). In that case, the Navier–Stokes

equation linearized around a mean flow $U_x(z) = -cz$, where c is a real constant, becomes

$$\frac{\partial u_i}{\partial t} + U_x \frac{\partial u_i}{\partial x} = -u_j \frac{\partial U_x}{\partial x_j} \delta_{i,x} - \partial_i p + \nu \nabla^2 u_i, \tag{B1}$$

where u_i is the i-th component of the velocity, ν is the kinematic viscosity, p is the fluid pressure (per unit density), and $\delta_{i,x}$ is the Kronecker delta. After Fourier-transforming Eq. (B1) using $u_i = \sum_{\mathbf{k}} a_i(k,t) \exp(i\mathbf{k} \cdot \mathbf{x})$, the evolution equation for the $\mathbf{k}$-th harmonic becomes

$$\frac{\partial a_i}{\partial t} + c \frac{\partial a_i}{\partial k_z} k_x = c a_z \delta_{i,x} - i k_i p - \nu k_j k_j a_i, \tag{B2}$$

where the Fourier-transformed p is determined using the incompressibility condition of the flow.

The amplitude-evolution equation (B2) is solved using the method of characteristics (a method which reduces a partial differential equation to a family of ordinary differential equations), yielding

$$\frac{da_i}{dt} = c a_z \delta_{i,x} - i k_i p - \nu k_j k_j a_i, \tag{B3}$$

where

$$\frac{d}{dt} \equiv \frac{\partial}{\partial t} + \frac{\partial k_j}{\partial t} \frac{\partial}{\partial k_j}. \tag{B4}$$

Comparing Eq. (B4) with Eqs. (B2) and (B3),

$$\frac{\partial k_j}{\partial t} \delta_{j,z} = c\, k_x. \tag{B5}$$

Equation (B5) predicts that the wavenumbers k_x and k_y do not change due to straining by the (x, y)-averaged mean shear flow—as expected.

However, since the mean shear flow does vary in z, the vertical scales of perturbations change over time due to the straining by the mean flow. Thus,

$$\frac{\partial k_z}{\partial t} = c\, k_x, \tag{B6}$$

which explains why all perturbations that vary along the direction of the mean flow (i.e., perturbations with $k_x \neq 0$) are strained by the mean flow, causing them to split apart in z after an appropriate eddy-straining time [28]. However, the x-invariant perturbations are not subjected to the eddy splitting, and thus those eddies are coherently stretched by the mean flow following the amplitude-evolution equation (B2). This is where the similarity between

the simple, local linear mean shear-flow and the KH-unstable non-local mean shear-flow ends; additional details are given in VI C in the main text.

[1] E.N. Parker, Hydromagnetic dynamo models, *Astrophys. J.* **122**, 293 (1955).

[2] A. Neronov and I. Vovk, Evidence for strong extragalactic magnetic fields from Fermi observations of TeV blazars, *Science* **328**, 73 (2010).

[3] R.M. Kulsrud, A critical review of galactic dynamos, *Annu. Rev. Astron. Astrophys.* **37**, 37 (1999).

[4] R.M. Kulsrud and E.G. Zweibel, On the origin of cosmic magnetic fields, *Rep. Prog. Phys.* **71**, 046901 (2008).

[5] A. Brandenburg, The case for a distributed solar dynamo shaped by near-surface shear, *Astrophys. J.* **625**, 539 (2005).

[6] S.M. Tobias, The turbulent dynamo, *J. Fluid Mech.* **912**, P1 (2021).

[7] J. Squire and A. Bhattacharjee, Generation of large-scale magnetic fields by small-scale dynamo in shear flows, *Phys. Rev. Lett.* **115**, 175003 (2015).

[8] K. Cline, N. Brummell, and F. Cattaneo, Dynamo action driven by shear and magnetic buoyancy, *Astrophys. J.* **599**, 1449 (2003).

[9] K. Cline, N. Brummell, and F. Cattaneo, On the formation of magnetic structures by the combined action of velocity shear and magnetic buoyancy, *Astrophys. J.* **588**, 630 (2003).

[10] A. Basu, S.A. Mao, A.A. Kepley, T. Robishaw, E.G. Zweibel, and J.S. Gallagher, Detection of an ∼20 kpc coherent magnetic field in the outskirt of merging spirals: the Antennae galaxies, *Mon. Not. R. Astron. Soc.* **464**, 1003 (2017).

[11] D.J. Price and S. Rosswog, Producing ultrastrong magnetic fields in neutron star mergers, *Science* **312**, 5774 (2006).

[12] G.M. Vasil, D. Lecoanet, K. Augustson, K.J. Burns, J.S. Oishi, B.P. Brown, N. Brummell, and K. Julien, The solar dynamo begins near the surface, *Nature* **629**, 769 (2024).

[13] K. Subramanian and A. Brandenburg, Traces of large-scale dynamo action in the kinematic stage, *Mon. Not. R. Astron. Soc.* **445**, 2930 (2014).

[14] P. Bhat, K. Subramanian, and A. Brandenburg, A unified large/small-scale dynamo in helical turbulence, *Mon. Not. R. Astron. Soc.* **461**, 240 (2016).

[15] P. Bhat, F. Ebrahimi, and E.G. Blackman, Large-scale dynamo action precedes turbulence in shearing box simulations of the magnetorotational instability, *Mon. Not. R. Astron. Soc.* **462**, 818 (2016).

[16] P. Bhat, Saturation of large-scale dynamo in anisotropically forced turbulence, *Mon. Not. R. Astron. Soc.* **509**, 2249 (2021).

[17] S.M. Tobias and F. Cattaneo, Shear-driven dynamo waves at high magnetic Reynolds number, *Nature* **497**, 463 (2013).

[18] M. Steenbeck, F. Krause, and K-H. Radler, *Z. Naturforsch.* **21a**, 369 (1966).

[19] A. Brandenburg, D. Elstner, Y. Masada, and V. Pipin, Turbulent processes and mean-field dynamo, *Space Sci. Rev.* **219**, 55 (2023).

[20] A. Pouquet, U. Frisch, J. Leorat, Strong MHD helical turbulence and the nonlinear dynamo effect, *J. Fluid Mech.* **77**, 321 (1976).

[21] B. Tripathi, A.E. Fraser, P.W. Terry, E.G. Zweibel, M.J. Pueschel, and R. Fan, Large-scale dynamos driven by shear-flow-induced jets, *Nature* **649**, 848 (2026).

[22] A. Yoshizawa, Self-consistent turbulent dynamo modeling of reversed field pinches and planetary magnetic fields, *Phys. Fluids B* **2**, 1589 (1990).

[23] S. Chandrasekhar, *Hydrodynamic and hydromagnetic stability* (Clarendon Press, Oxford 1961).

[24] D. Lecoanet, M. McCourt, E. Quataert, K.J. Burns, G.M. Vasil, J.S. Oishi, B.P. Brown, J.M. Stone, and R.M. O'Leary, A validated non-linear Kelvin-Helmholtz benchmark for numerical hydrodynamics, *Mon. Not. R. Astron. Soc.* **455**, 4274 (2016).

[25] G.K. Batchelor, On the spontaneous magnetic field in a conducting liquid in turbulent motion, *Proc. R. Soc. London, Ser. A* **201**, 405 (1950).

[26] G.K. Batchelor and I. Proudman, The effects of rapid distortion of a fluid in turbulent motion, *Q. J. Mech. Appl. Math.* **7**, 83 (1954).

[27] A.A. Townsend, *The structure of turbulent shear flow*, 2nd Ed. (Cambridge University Press, Cambridge, 1976).

[28] P.W. Terry, Suppression of turbulence and transport by sheared flow, *Rev. Mod. Phys.* **72**, 109 (2000).

[29] K.M. Smith, C.P. Caulfield, and J.R. Taylor, Turbulence in forced stratified shear flows, *J. Fluid Mech.* **910**, A42 (2021).

[30] J.B. Marston, E. Conover, and T. Schneider, Statistics of an unstable barotropic jet from a

cumulant expansion, *J. Atmos. Sci.* **65**, 1955 (2008).

[31] L. Cope, P. Garaud, and C. Caulfield, The dynamics of stratified horizontal shear flows at low Péclet number, *J. Fluid Mech.* **903**, A1 (2020).

[32] M.J. Pueschel, F. Jenko, D. Told, and J. Büchner, Gyrokinetic simulations of magnetic reconnection, *Phys. Plasmas* **18**, 112102 (2011).

[33] M.J. Pueschel, D. Told, P.W. Terry, F. Jenko, E.G. Zweibel, V. Zhdankin, and H. Lesch, Magnetic reconnection turbulence in strong guide fields: Basic properties and application to coronal heating, *Astrophys. J. Suppl. Ser.* **213**, 30 (2014).

[34] B. Tripathi, A.E. Fraser, P.W. Terry, E.G. Zweibel, and M.J. Pueschel, Mechanism for sequestering magnetic energy at large scales in shear-flow turbulence, *Phys. Plasmas* **29**, 070701 (2022).

[35] B. Tripathi, P.W. Terry, A.E. Fraser, E.G. Zweibel, and M.J. Pueschel, Three-dimensional shear-flow instability saturation via stable modes, *Phys. Fluids* **35**, 105151 (2023).

[36] A. Elias-López, F.D. Sordo, and D. Viganò, Vorticity and magnetic dynamo from subsonic expansion waves, *Astron. Astrophys.* **677**, 46 (2023).

[37] P.W. Terry, Inverse energy transfer by near-resonant interactions with a damped-wave spectrum, *Phys. Rev. Lett.* **93**, 235004 (2004).

[38] P.W. Terry, Zonal Flows in Magnetically Confined Plasmas: Theory, in Zonal Jets, Boris Galperin and Peter L. Read, editors, p. 181-193 (Cambridge University Press, London 2019).

[39] B. Galperin, H. Nakano, H.-P. Huang, and S. Sukoriansky, The ubiquitous zonal jets in the atmospheres of giant planets and Earth's oceans, *Geophys. Res. Lett.* **31**, L12203 (2004).

[40] S. Tobias and F. Cattaneo, Limited role of spectra in dynamo theory: coherent versus random dynamos, *Phys. Rev. Lett.* **101**, 125003 (2008).

[41] A.A. Schekochihin, J.L. Maron, S.C. Cowley, and J.C. McWilliams, The small-scale structure of magnetohydrodynamic turbulence with large magnetic Prandtl numbers, *Astrophys. J.* **576**, 806 (2002).

[42] J. Maron, S. Cowley, and J. McWilliams, The nonlinear magnetic cascade, *Astrophys. J.* **603**, 569 (2004).

[43] W.M. Elsässer, The Hydromagnetic Equations, *Physical Review* **79**, 183 (1950).

[44] K.J. Burns, G.M. Vasil, J.S. Oishi, D. Lecoanet, and B.P. Brown, Dedalus: A flexible framework for numerical simulations with spectral methods, *Phys. Rev. Research* **2**, 023068 (2020).

[45] M.K. Verma, *Energy transfers in fluid flows: multiscale and spectral perspectives* (Cambridge University Press, Cambridge 2019).

[46] N.K. Singh, I. Rogachevskii, and A. Brandenburg, Enhancement of Small-scale Turbulent Dynamo by Large-scale Shear, *Atrophys. J. Lett.* **850**, L8 (2017).

[47] B. Tripathi, A.E. Fraser, P.W. Terry, E.G. Zweibel, and M.J. Pueschel, Near-cancellation of up- and down-gradient momentum transports in magnetized shear flow turbulence due to stable modes, *Phys. Plasmas* **29**, 092301 (2022).

[48] D. Biskamp, *Magnetohydrodynamic turbulence* (Cambridge University Press, 2003).

[49] I.G. Cresswell, E.H. Anders, B.P. Brown, J.S. Oishi, and G.M. Vasil, Force balances in strong-field magnetoconvection simulations, *Phys. Rev. Fluids* **8**, 093503 (2023).

[50] B. Tripathi, A.E. Fraser, P.W. Terry, E.G. Zweibel, M.J. Pueschel, and E.H. Anders, Nonlinear mode coupling and energetics of driven magnetized shear-flow turbulence, *Phys. Plasmas* **30**, 072107 (2023).

[51] P. Garaud, Double-Diffusive Convection at Low Prandtl Number, *Annu. Rev. Fluid Mech.* **50**, 275 (2018).

[52] A.E. Fraser, S.A. Reifenstein, and P. Garaud, Magnetized Fingering Convection in Stars, *Astrophys. J.* **964**, 184 (2024).

[53] U.M. Ascher, S.J. Ruuth, and R.J. Spiteri, Implicit-explicit Runge-Kutta methods for time-dependent partial differential equations, *Appl. Numer. Math.* **25**, 151 (1997).

[54] D. Wang and S.J. Ruuth, Variable step-size implicit-explicit linear multistep methods for time-dependent partial differential equations, *J. Comput. Math.* **26**, 838 (2008).

[55] A.E. Fraser, P.W. Terry, E.G. Zweibel, and M.J. Pueschel, Coupling of damped and growing modes in unstable shear flow, *Phys. Plasmas* **24**, 062304 (2017).

[56] B.F. Farrell and P.J. Ioannou, Dynamics of streamwise rolls and streaks in turbulent wall-bounded shear flow, *J. Fluid Mech.* **708**, 149 (2012).

[57] P.W. Terry, A.S. Ware, and D.E. Newman, Relaxation oscillations induced by amplitude-dependent frequency in dissipative trapped electron mode turbulence, *Phys. Plasmas* **1**, 3974 (1994).

[58] B. Tripathi, D. Nandy, and S. Banerjee, Stellar mid-life crisis: subcritical magnetic dynamos of solar-like stars and the breakdown of gyrochronology, *Mon. Not. R. Astron. Soc. Lett.* **506**, 50 (2021).

[59] A.L. Wilmot-Smith, D. Nandy, G. Hornig, and P.C.H. Martens, A time delay model for solar and stellar dynamos, *Astrophys. J.* **652**, 696 (2006).

[60] A. Seta, P.J. Bushby, A. Shukurov, and T.S. Wood, Saturation mechanism of the fluctuation dynamo at $\mathrm{Pr_M} \geq 1$, *Phys. Rev. Fluids* **5**, 043702 (2020).

[61] S.A. Olausen and V.M.Kaspi, The McGill magnetar catalog, *Astrophys. J. Suppl. Ser.* **212**, 6 (2014).

[62] A. Bahramian and N. Degenaar, *Low-mass X-ray binaries* (Springer Nature, Singapore, 2022), pp. 1–62.

[63] K. Kiuchi, P. Cerdá-Durán, K. Kyutoku, Y. Sekiguchi, and M. Shibata, Efficient magnetic-field amplification due to the Kelvin-Helmholtz instability in binary neutron star mergers, *Phys. Rev. D* **92**, 124034 (2015).

[64] T.G. Cowling, The magnetic field of sunspots, *Mon. Not. R. Astron. Soc. Lett.* **94**, 39 (1933).

[65] Ya. B. Zeldovich, *Zh. Eksp. Teor. Fiz.* **31**, 154 (1956) [*Sov. Phys. JETP* **4**, 460 (1957)].

[66] B. Tripathi, A.J. Barker, A.E. Fraser, P.W. Terry, and E.G. Zweibel, Predicting the slowing of stellar differential rotation by instability-driven turbulence, *Astrophys. J.* **966**, 195 (2024).

[67] F. Waleffe, Inertial transfers in the helical decomposition, *Phys. Fluids A* **5**, 677 (1993).

[68] L.M. Smith and F. Waleffe, Transfer of energy to 2D large scales in forced, rotating 3D turbulence, *Phys. Fluids* **11**, 1608 (1999).

[69] L.M. Smith and F. Waleffe, Generation of slow, large scales in forced, rotating, stratified turbulence, *J. Fluid Mech.* **451**, 145 (2002).

[70] J.J. Riley and M.-P. Lelong, Fluid motions in the presence of strong stable stratification, *Annu. Rev. Fluid Mech.* **32**, 613 (2000).

[71] D. Biskamp and A. Zeiler, Nonlinear instability mechanism in 3D collisional drift-wave turbulence, *Phys. Rev. Lett.* **74**, 706 (1995).

[72] C. Ng and A. Bhattacharjee, Interaction of shear-Alfven wave packets: implication for weak magnetohydrodynamic turbulence in astrophysical plasmas, *Astrophys. J.* **465**, 845 (1996).

[73] S. Du, H. Li, X. Fu, and Z. Gan, Anisotropic Energy Transfer and Conversion in Magnetized Compressible Turbulence, *Astrophys. J.* **948**, 72 (2023).

[74] F. Rincon, Dynamo theories, *J. Plasma Phys.* **85**, 205850401 (2019).

[75] V. Skoutnev, J. Squire, and A. Bhattacharjee, On large-scale dynamos with stable stratification and the application to stellar radiative zones, *Mon. Not. R. Astron. Soc. Lett.* **517**, 526

(2022).

[76] M.R.E. Proctor, Bounds for growth rates for dynamos with shear, *J. Fluid Mech.* **697**, 504 (2012).

[77] E.R. Most, Impact of a mean field dynamo on neutron star mergers leading to magnetar remnants, *Phys. Rev. D* **108**, 123012 (2023).

[78] D. Radice, General-relativistic Large-eddy Simulations of Binary Neutron Star Mergers, *Astrophys. J. Lett.* **838**, L2 (2017).

[79] R. Aguilera-Miret, D. Viganò, and C. Palenzuela, Universality of the Turbulent Magnetic Field in Hypermassive Neutron Stars Produced by Binary Mergers, *Astrophys. J. Lett.* **926**, L31 (2022).

[80] K. Kiuchi, A. Reboul-Salze, M. Shibata, and Y. Sekiguchi, A large-scale magnetic field produced by a solar-like dynamo in binary neutron star mergers, *Nat. Astron.* **8**, 298 (2024).

[81] D.W. Hughes and M.R.E. Proctor, Large-scale Dynamo Action Driven by Velocity Shear and Rotating Convection, *Phys. Rev. Lett.* **102**, 044501 (2008).

[82] S. Biswas and R. Ganesh, Effect of flow shear on the onset of dynamos, *Phys. Plasmas* **30**, 112902 (2023).

[83] A.E. Fraser, M.J. Pueschel, P.W. Terry, and E.G. Zweibel, Role of stable modes in driven shear-flow turbulence, *Phys. Plasmas* **25**, 122303 (2018).

[84] S.G.L. Smith and S.M. Tobias, Vortex dynamos, *J. Fluid Mech.* **498**, 1 (2004).